

Reduced Order Thermal Simulation of Lithium-Ion Battery Packs

Sam Thomas

*Department of Aeronautical and Automotive Engineering,
Loughborough University, Leicestershire LE11 3TU, UK*

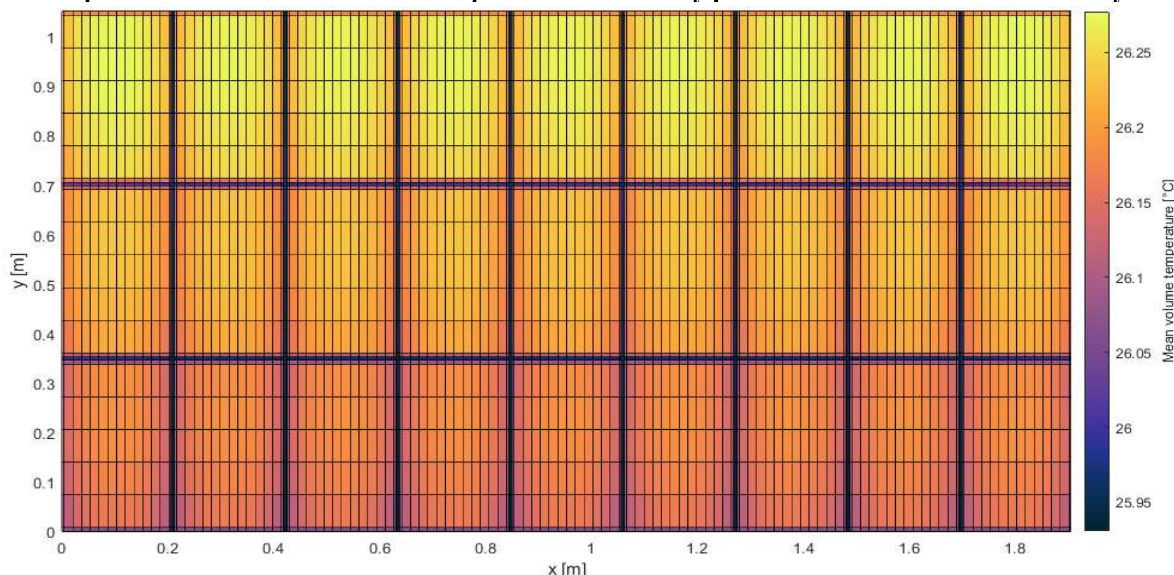
Abstract

To reduce full battery pack modelling computational and setup time, a fully configurable electrical and thermal battery pack model has been produced in Simulink and a reduced order form of the model has been tested with promising results. Computational speed was improved by 80% from 34 to 169 times real-time using a reduced order state-space implementation of the model based on a principal component analysis of the results. Reduced order accuracy was very high within the ambient cooling region of the pack. However, it was unable to effectively model the pack when active cooling was in use, this is a key area for future work.

The electrical model uses a look-up table based single resistor-capacitor pair equivalent circuit model (ECM). Cell currents are determined using the total pack power requirement. The thermal model uses finite volume methods and insulation boundary conditions to solve the heat diffusion equation across the pack. Boundary thermal conductivities are assumed as a combination of conduction and linearised black-body radiation. For configurability an extensive initialisation function defines parameters based on inputs for derived matrix form equations that describe the performance of the pack. This contains complex loops to define matrices containing indices used during runtime, as this looping is not required during runtime, performance is improved. For realistic performance of the model, basic control and thermal management modelling has been implemented, allowing active and passive cooling modelling.

The pack structure is based on a skateboard chassis with modules of pouch cells arranged in a grid structure. This is a common approach in the automotive industry currently in use by multiple manufacturers. Specifically, due to the availability of specifications, the model layout is based on the Audi e-tron pack design.

Graphical abstract: Mean volume temperature of a battery pack after three consecutive drive cycles



*Automotive Engineering MEng; B723936; Project supervisor: Dr Thomas Steffen

1. Introduction

Increased regulatory pressure in efforts to reduce greenhouse gas emissions [1] has been a driving factor in the push for more environmentally friendly transportation. On top of these regulations, multiple governments have provided funding and policies, such as subsidies [2], to support the development process and aid the purchase of battery electric vehicles (BEVs) by consumers. Due to this, demand for BEVs is growing rapidly. Large efforts from industry leaders to meet this demand has resulted in massive innovation in battery technology, motors, and control. Because of these innovations, BEVs are becoming a viable alternative to internal combustion engine (ICE) vehicles for an increasing number of consumers.

Lithium-ion batteries have been a key technology at the forefront of this industry shift. Energy density and cost of Lithium-ion cells has been improving rapidly, with the real price per energy capacity decreasing by 13% per year between their commercial introduction in 1992 and 2016 [3]. Despite this, due to their relatively new adoption and expensive raw materials in comparison to ICEs they are still one of the most expensive parts of a BEV and need to last for the lifetime of the vehicle for it to be commercially viable.

Degradation is a large obstacle to this, reducing the lifetime of battery packs. Cyclic and calendar ageing reduce the performance and capacity of battery packs over time, leading to short lifetimes when compared to ICEs. The operating temperature envelope of a lithium-ion cell heavily effects the rate of degradation and performance. Typically, the ideal range is from $10 - 35^{\circ}\text{C}$, with a target temperature around 25°C . Operating above or below this desired range leads to elevated rates of irreversible capacity loss and degradation [4]. Undesired side reactions lead to a loss of lithium inventory as it is reacted in between the anode and cathode. Generally, the rate of these reactions follows an Arrhenius relationship, with an exponential increase in the rate constant as temperature increases, this means small increases above the desired temperature can result in large increases in the degradation rate. Additionally, the temperature distribution in the pack is another very important factor when considering degradation. Non-uniform temperature distribution can have a drastic effect on the degradation of specific cells in the pack [5]. The pack capacity is heavily limited by the lowest capacity cell when uneven degradation occurs, if charging continues past this point the degraded cell may exceed upper voltage limits. This causes lithium plating on the anode; in extreme cases the plating can cause internal short-circuits in the cells and subsequent rapid heating. During this heating, if the cell reaches 90°C the solid electrolyte interface layer starts to decompose and self-heating reactions start, leading to a thermal runaway [6]. This runaway can propagate through the pack if neighbouring cells are heated, leading to a catastrophic error. These factors emphasise the importance of capable cooling solutions and their subsequent control methods to maintain ideal temperatures uniformly across the whole pack. Identifying the need for work that is aimed to improve the design process, such as this study.

To maintain the target temperature across the pack at a large range of ambient temperatures complex thermal management systems and control strategies are required. Complex control and accurate modelling of thermal management systems is out of the scope of this work. Instead of implementing complete system level models containing additional components such as power electronics, motors, and cabin, the main goal of the battery model is for it to be placed in a library and implemented into a system level thermal management model. The pack model would receive a coolant input temperature and flow rate as well as a drive cycle or power demand, from this the pack model will output cell temperatures and a coolant output temperature. The output coolant would then be used for the wider system thermal model and the cell temperature output can be implemented into the system control. In this work the model is not being used for this purpose yet, so some control and thermal management modelling is required for representative performance of the pack over a drive cycle. For this purpose, basic

*Automotive Engineering MEng; B723936; Project supervisor: Dr Thomas Steffen

control and lookup-table based radiator and refrigerant loop models for active and passive cooling have been implemented at this stage.

During the battery pack design process, full scale pack modelling is crucial for evaluating the performance of different cooling or control solutions without the need for expensive prototypes. Modelling the full thermal performance of a pack generally involves the production of detailed models, most commonly finite volume or finite element models, these require the parameterisation of individual volumes/elements and the interactions between them. For realistic performance, an electrical model must also be implemented to determine reasonable heat generation during pack operation. The resulting combined model is generally high order with a very large number of states, resulting in slow simulations. On top of this, if the pack layout is changed, redefining the finite model is time consuming.

The core aim of the project is to provide a more convenient alternative for full-scale electrical and thermal battery pack modelling, implementing equation generation based on user inputs for easy reconfiguration and model order reduction for faster than real-time pack level simulations. It aims to provide the temperature, state of charge (SOC), open circuit voltage (OCV) and some basic degradation metrics for each cell. The target use case for this model is in rapid testing of initial thermal management system configurations and control strategy development. It will allow fast testing of different configurations quickly for use in key initial decisions in the design process. Examples of this include the number of cells in a module and their orientation with respect to the global coordinates, how the modules are stacked and coolant flow direction.

User inputs for the pack layout, thermal configuration and simulation are retrieved, defining key parameters for the electrical and thermal configuration of the pack. From these inputs, relevant parameters for generalised functions can be formulated during the initialisation, describing processes including heat generation, cell loading and heat transfer. All equations have been derived in matrix form, allowing for wide range of implementations.

The model in this study is based on a common battery pack structure in current BEVs. This is the skateboard structure, where modules containing 10 – 20 stacked lithium-ion pouch cells are arranged in a grid like pattern. Parameters from the Audi e-tron 55 quattro are used for the base pack layout in the order reduction testing and sensitivity analysis. Although the initialisation function for the model is based on this pack layout, other model structures could be implemented with small changes to the code.

Where possible, simplifications to the model are made to avoid excess states and complexity when it is not required. For example, although the cells are modelled thermally as multiple volumes, heat generation is assumed to be uniform over the cell. This approach has a two-fold effect on the model, simplified equations aid the equation generation process and at model runtime solving the equations is generally less computationally intensive, improving the speed of the model. Another argument for simplification is that it allows this stage of the process to be a proof of concept to the wider methods of the model. If this attempt is successful, more complex equations can be implemented using the same technique, potentially providing a more powerful final tool.

The structure of the report is as follows. First an overview of key literature for the project are provided. Following this, the aims and methodology of the work are shown. Next, a detailed look at the model formation process is provided, discussing the key areas of the model separately. After this, the order reduction process is discussed and a sensitivity analysis is completed on the original model, highlighting key areas for parameterisation. Finally, beneficial future work is overviewed, and conclusions are made related to the overall aims of the work.

2. Literature Review

2.1. Thermal model

2.1.1. Modelling method

There are three main modelling approaches for thermal battery models, reviewed in [7], these are lumped capacitance models, numerical and analytical models, and ECMs. Figure 1 shows a summary of the comparison of these methods from [7]. In this application, electrical behaviour modelling is required, and fast processing time is desired. This suggests that an ECM thermal model is a good fit. However, to compare the performance of cooling methods and display temperature gradients, more detailed thermal modelling is required, this is not provided by an ECM as cell temperature is assumed as uniform. The solution used in this model is a combination of ECM and numerical modelling, an ECM is used to determine heat generation based on a mean temperature provided by the numerical model.

Figure 1: Thermal modelling method comparison – Reproduced from [7]

Method	Advantages	Disadvantages	Recommended Applications
Lumped Capacitance Thermal Models	Simple as parameters are lumped into capacitance Quick to design and run	Physical constraints due to B_i number limitations Inaccuracies in extreme operating conditions	System level modelling with fast processing time Under normal conditions
Numerical and Analytical Thermal Models	Not very complex but yields good levels of accuracy Implement heterogeneity with more computational time	Requires accurate representation of chemical and material compositions Computationally intensive Inflexible and specific to the battery being designed	Where high accuracy is required Ideal for cell level modelling Useful tool for system design optimisation
Equivalent Circuit Thermal Models	Faster, more flexible, and easier to formulate than numerical Minimal computational effort is required	Potentially less accurate as the model calculates an average temperature for the entire chemistry	System level modelling with fast processing time Compact thermal management systems When electrical behaviour modelling is also required

An overview and examples of different numerical methods used in battery thermal modelling is provided in [7], all the methods use differential equations to solve for energy balance. The two methods considered for this study were finite element methods (FEM) and finite volume methods (FVM), they both divide the body into segments and define thermal parameters to each segment and global boundary conditions to solve the heat diffusion equation. FVM models are becoming increasingly popular for complex thermal simulations, a key example of this is computational fluid dynamics (CFD), for example a CFD model for the thermal analysis of lithium-ion modules with air cooling is produced in [8]. Alternatively, [9] used FEM with the fundamental principles of heat transfer to analyse the thermal management of thin film lithium-ion batteries. An overview of the key features of FVM in comparison to FEM is provided in [10]. They state that the local conservativity of numerical fluxes is a feature that makes FVM more attractive than FEM for thermal applications. This means that flux is conserved between adjacent cells, this is effective for solving diffusion-based problems, hence the common use of FVM in thermal problems. Due to this, FVM is used for the model.

2.1.2. Heat generation

Battery heat generation is a combination of ohmic and entropic heat generation. Due to low contributions (5 – 10% [11]), entropic heat generation is ignored in this work as the increase in complexity is not warranted, this method is used in [8]. Additionally, heat generation is considered as a volume average heat source for simplicity, this approach is used in the CFD model in [12].

2.1.3. Material properties

For the FVM model, the specific heat capacity, density, and thermal conductivity need to be defined for each material in the pack. Only three materials are considered in this stage, nickel manganese cobalt (NMC) lithium-ion cell material, aluminium and 50/50 ethylene glycol coolant. Parameters for aluminium and the coolant are readily available on websites such as the engineering toolbox [13].

Although these thermal parameters vary with temperature, due to the relatively narrow operating temperature region of a lithium-ion battery, these variations tend to be small. On a graph of density against temperature, the change in density for aluminium is barely noticeable between $200 - 400K$ [14]. Also, the variation of aluminium thermal conductivity from $200 - 400K$ is $\sim 1\%$ [15]. Ethylene glycol has higher variations; however, they are still low enough to justify the simplistic approach. From $0 - 40^\circ C$ specific heat capacity and density vary by $\sim 3.5\%$ and $\sim 2\%$ respectively [16].

Cell density has been calculated using the dimensions and mass of an example cell used in the Audi e-tron from [17].

Cell specific heat capacity appears to vary in the literature so an average value has been found from multiple studies, [18], [19], [11], [20] give values of 950, 1138, 1112 and $1150 J kg^{-1} K^{-1}$ respectively. Averaging these results in 1087.5, this has been rounded up to 1100 as 950 appears to be more of an outlier.

Due to the layered structure of the cell material, the thermal conductivity is anisotropic. Thermal conductivity in-plane is high, where heat transfer is dominated by the high conductivity of aluminium and copper current collectors. Alternatively, cross-plane or through the thickness conductivity is low, heat transfer is limited by the low conductivity separators. Two equations calculating the in-plane and through the thickness thermal conductivity are defined in [21] using the unit cell approach, which defines the cell as a cube consisting of the smallest repetition of the cell layers. The uncertainty of these equations was evaluated in [21] using data from the literature for temperature/pressure dependence of the conductivities of the stacked materials, as well as a common uncertainty in micrometre measurements. The uncertainty of in-plane and cross-plane thermal conductivities were calculated as 6% (0.371 to $1.254 W m^{-1} K^{-1}$) and 58% (24.7 to $28.3 W m^{-1} K^{-1}$) respectively, logically the cross-plane uncertainty is larger as the heat must transfer through all layers.

Unlike the aluminium and coolant thermal properties, cell material properties change with respect to temperature and SOC, resulting in higher potential variations. Varying the SOC from $0 - 1$ and the temperature from $0 - 40^\circ C$ for an NMC pouch cell resulted in a thermal conductivity change of $\sim 5\%$ [20]. The data from [21] suggests that SOC has a large impact on this mechanic. It shows the variation of thermal conductivity between $0 - 40^\circ C$ for two NMC cells with different external pressures is $\sim 1.5 - 2\%$, less than half the change shown in [20]. Specific heat capacity does experience much larger changes, over the same conditions as above, [20] shows a variation of $\sim 21\%$. Although not used in this study, this could warrant the implementation of a varied specific heat capacity. It could provide interesting results regarding temperature gradients. As a cell's temperature increases, its heat capacity goes up, this would then inhibit further temperature increases, potentially reducing temperature gradients in the pack as cooler cells heat quicker to match hotter cells.

Additionally, during normal operation of the model these variations will be smaller as the full temperature and SOC ranges will not be used. For example, using the model produced in this study, a single worldwide harmonised light vehicle test cycle (WLTC) with an ambient temperature of $20^\circ C$, initial SOC of 0.95, and no cooling had a maximum cell temperature of $22^\circ C$ and minimum SOC of 0.85. Based on the data in [20], the estimated specific heat capacity change would be below 1%. As a result of this, it is believed that the assumption of constant thermal properties is valid at this stage.

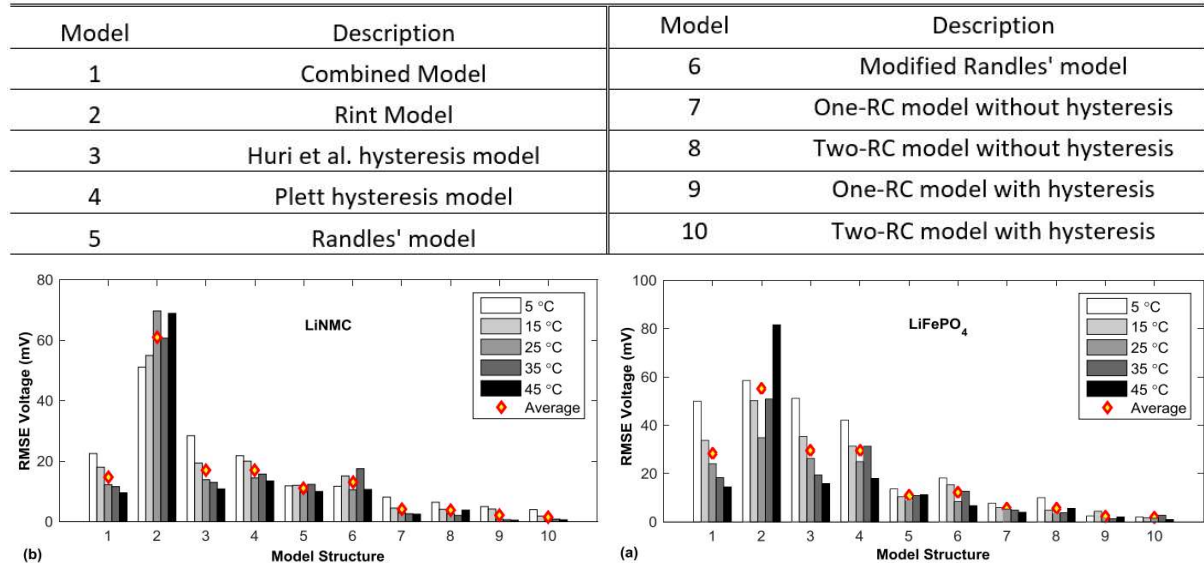
*Automotive Engineering MEng; B723936; Project supervisor: Dr Thomas Steffen

2.2. Electrical model

2.2.1. Equivalent circuit model

[22] provides a systematic review of ECMs for real-time battery state estimation. 10 different models are constructed, and the root mean square voltage errors against experimental data from an NMC, and lithium iron phosphate (LFP) cell are compared, the results of this are shown in Figure 2. Based on these results, the 1RC (Model 7) was selected as it provides a good balance of accuracy and complexity. The 1RC model contains a controlled voltage source (OCV), a series resistance and a parallel resistor-capacitor (RC) pair, used to represent overpotential [23]. Accuracy can be improved with hysteresis modelling or an additional RC pair, however as shown in [22], the accuracy improvement is small. For adaptability, in future work, the choice between 1RC, 2RC and a single resister could be implemented. This will allow improved accuracy/transient response if required and allow transients to be negated if unnecessary, e.g. long term degradation modelling [24]. Parameters from the 2RC model in [25] are used for this work. It contains 2D lookup tables for each parameter as a function of SOC and temperature from a 32Ah NMC/Graphite cell.

Figure 2: Comparison of equivalent circuit models from [22]



2.2.2. State of charge

SOC estimation methods can be divided into five strategies, coulomb counting, OCV method, impedance spectroscopy-based, model-based, and artificial neural network-based, reviewed in [26]. Coulomb counting is the simplest method using a direct integration of current to calculate the SOC. Accuracy is dependent on the initial SOC measurement and accumulated current measurement errors. In this case initial SOC and current for each cell will be clearly defined in the model. Due to this, coulomb counting is used for SOC measurement.

For improved accuracy, some models account for coulombic efficiency (CE), for example [22]. However, as lithium ion cells have very high CE, (99.90% for LCO [27]) CE is assumed to be 100%.

2.3. Pack configuration

To determine an appropriate approach to the base pack layout, a review of different battery pack types in industry was completed. It was found that liquid cooling was almost exclusively used over air cooling and that base plate cooling was a popular approach to this. Currently pouch cells are much more popular in industry, almost all manufacturers apart from Tesla and Rivian are using pouch cells, with some other use of prismatic cells. These are commonly arranged in modules of 10 – 20 cells in a skateboard like chassis. Due to these findings, the model will focus on pouch cells in this configuration as it is relevant to industry.

The Audi e-tron [17] uses modules of 12 pouch cells in a 4 series, 3 parallel (4S3P) configuration. Modules are arranged in a grid in a skateboard chassis with base plate cooling. The BMW gen5 [28] pack is another example of a similar configuration with a skateboard chassis and base cooling. This uses next generation solid-state batteries, indicating that this configuration will continue to be used in the future. The Jaguar I-Pace [29] has another similar configuration with a skateboard chassis and with what appears to be baseplate cooling. The VW ID.4 [30] uses 8 – 12 modules, each containing 24 pouch cells, these are arranged in another similar structure and use baseplate cooling. Finally, the Chevrolet Bolt [31] has another similar structure. These extensive examples justify the decision to base the model on this configuration type.

Specifically, due to the availability of configuration information, including cell dimensions and detailed images of the pack layout (Figure 7), the model will be based on the Audi e-tron prior to the change from pouch to prismatic cells in January 2021.

2.4. Order reduction

To reduce the order of the thermal model, trends in the results need to be found and simplified based on inputs to the system such as coolant temperature and heat generation. A common approach to this is a form of multivariate statistical technique. Principal component analysis (PCA) is a popular type of this. [32] describes this method in detail, PCA involves analysing a data table of observations described by multiple dependent variables. The goal of this method is extracting information from the data and expressing it as a set of orthogonal variables known as principal components. Coefficients are defined for each of these components which can be used to reconstruct the full data set from the components.

PCA has been used in various applications relating to lithium-ion batteries. [33] uses PCA along with multivariate adaptive regression splines (MARS) to develop a predictive model for SOC. Also [34] uses a functional PCA to decompose degradation signals for use in degradation modelling.

Mathworks provide a robust PCA function [35] within the statistics and machine learning toolbox in Matlab that completes all the calculations to extract the principal components from raw data. Producing the required parameters for implementation of PCA in this work.

3. Aims and Objectives

The core aim of the project is to establish a robust full-scale electrical and thermal battery pack model and implement model order reduction techniques to improve computational time while maintaining accuracy.

Objectives for the project are listed below, dividing the core aim, these will be monitored during the project and evaluated after work is completed for performance evaluation.

- Create a base battery pack model with reasonable accuracy that will allow the investigation of the proposed order reduction method.
- Produce an initialisation script that generates electrical and thermal equations for the model based on pack configuration inputs, allowing for rapid changes in test configuration without the need to redesign the model.
- Implement a reduced order version of the model with reasonable accuracy and the capability of real-time simulation due to computational savings.
- Perform a sensitivity analysis of key parameters in the model with large uncertainty, identifying important areas for parameterisation of the model for experimental data.
- If possible, integrate the impact of degradation on the impedance of the cells for more robust degradation analysis. This is an additional aim that should be considered based on the speed of progression of the project.

4. Methodology

Due to the large number of components in the model it was not feasible to attempt to create the full model in one stage. First, a work breakdown structure (WBS) was produced, providing a comprehensive division of the project into stages and their individual tasks. After this, an extensive weekly Gantt chart was produced to show the work order, task duration and dependencies. Mitigations for the main risks were considered and contingency plans were implemented in case of failed work.

The main approach to the project was to provide consistent progression in complexity with key milestones to validate work. An example of this was the implementation of the electrical model in Simulink, first a single-cell model was produced and validated against existing circuit simulation software. Next, the model was expanded to the module level and again validated. Finally, it was expanded again to the pack level and validated. This approach ensures errors are caught early and do not propagate into later work.

Some of the key milestones for the work are shown below. Note that this is not an exhaustive list and the progression through these milestones was not linear. Parallel work was completed to progress to different milestones simultaneously. An example of this is that the electrical and thermal models were completed in steps concurrently, progressing from the cell level to module and finally pack level. Although degradation modelling is included on the stages and within the aims, due to time restraints during the project, degradation was not considered in the model at this stage so will not be covered in the model formation.

1. Vehicle model completion
2. Pack level electrical model completion
3. Pack level thermal model completion
4. Combination of vehicle, electrical and thermal models
5. Implementation of battery thermal management
6. Implement equation generation based on user configuration
7. Successful order reduction of full pack model
8. Degradation modelling implemented

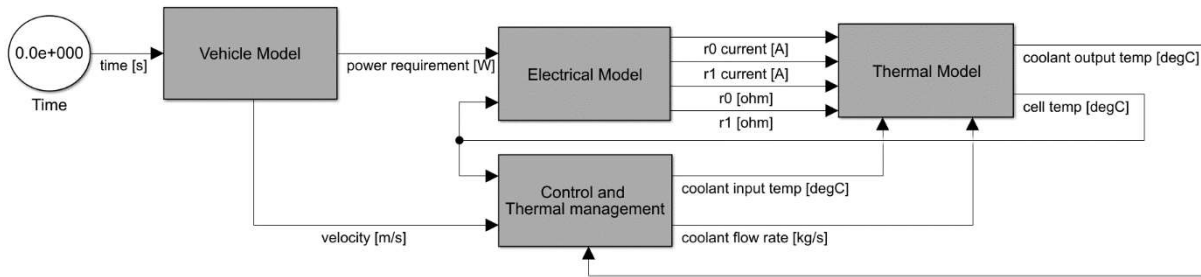
5. Model formulation

The model has been divided into four key areas, these are the vehicle model, electrical model, thermal model and finally the control and thermal management.

A vehicle model calculates power demand based on a drive cycle. Individual cell currents are then determined within the electrical model using this power requirement. Heat generation is then calculated using the cell current and resistances in the thermal model. Based on a basic control principle, heat rejection through cooling and heat flux due to coolant flow is determined in the control and thermal management block. Using these and the thermal configuration the heat diffusion equation can be solved, producing cell and output coolant temperatures for the next step.

The full model and all initialisation files are provided in a GitHub repository [36].

Figure 3: Simulink model overview



5.1. Vehicle model

To determine the pack power requirement a basic vehicle model has been produced based on the 2021 Audi e-tron 50 quattro, see Table 1 for parameters. It uses a lookup table from a given drive cycle to get the vehicle velocity, in this study the WLTC cycle has been used. Velocity is then used to calculate the power demand using Equation 1 where v is the vehicle velocity and t is time. It combines the inertial, drag and rolling resistance forces and multiplies them by the velocity to get the power requirement. To provide a reasonable power for smaller/larger packs when varying the model configuration, power demand is scaled linearly with the ratio of the model and e-tron pack energies. It is important to reduce power demand on smaller packs as inaccessible power demands will lead to imaginary solutions to the quadratic pack current equation (Equation 3).

$$P = v \left(\frac{1}{2} \rho v^2 C_d A_f + M g (v A_d + B_d) + M \frac{dv}{dt} \right) \cdot \frac{E_{model}}{E_{etron}} \quad 1$$

Table 1: Vehicle model parameters

Parameter	Value
Air density (ρ)	1.225 kg m^{-3} (constant)
Drag co-efficient (C_d)	0.28 [37]
Frontal area (A_f)	3.15 m^2 [37]
Vehicle mass (M)	2565 kg [37]
Acceleration due to gravity (g)	9.81 ms^{-2} (constant)
Static rolling resistance co-efficient (A_d)	0.011 (assumed)
Dynamic rolling resistance co-efficient (B_d)	0.001 (assumed)
Cell energy (E_{cell})	220 Wh [17]
Model pack energy (E_{model})	Based on configuration and cell energy
E-tron pack energy (E_{etron})	71 kWh [37]

5.2. Electrical model

5.2.1. Cell model

The electrical cell model is a single RC pair ECM, this is shown in Figure 5. The first resistor (R_0) represents the ohmic resistance in the cell, accounting for the electrode and electrolyte ionic conductivities as well as the current collector resistance. The RC pair containing R_1 and C_1 represents the low-speed transients in the cell, mainly double-layer capacitance at the electrode/electrolyte boundaries caused up by the build-up of ions. A voltage and current supply represent the OCV and load current on the cell respectively.

The parameterised 2RC parameters from [25] are from a 32Ah NMC/Graphite cell. The 32Ah parameters need to be scaled for the 60Ah cells used in the e-tron so heat generation is representative. Both cells use the same chemistry and are designed for similar applications, so it is assumed the construction of the cells is the same, including electrode layer thicknesses and materials. This means the active material area between the cells will scale linearly with the capacity, a 1.875 (60/32) times increase. As the area for ion transfer increases, resistance reduces. Also, a larger number of ions are deposited at the electrode/electrolyte boundaries, increasing the double layer capacitance. The resistances and capacitance have been divided and multiplied by 1.875 respectively, maintaining the transient response of the cell, as the time constant of the RC pair is the product of the resistance and capacitance. This is supported by the equations for resistance and capacitance, they are inversely proportional and proportional to area respectively.

The cells are modelled using the Simulink based approach shown in [38]. R_0 current is simply the cell input current; this is calculated using the pack power demand below. Transient response is calculated without an algebraic loop by integrating the current over the capacitor, producing charge, then using the capacitance to calculate voltage. With this voltage the distribution of current between R_1 and C_1 can be calculated. This approach has been validated against an equivalent Simscape model with capacitor and resistor blocks.

5.2.2. Cell loading

Individual cell currents must be determined using the total power demand. For a single cell, power (P) is calculated using Equation 2 where I_{cell} is the cell current and V_{ocv} and V_1 are the OCV and RC voltages respectively. Equation 3 shows this equation in quadratic form.

$$P = I_{cell}((V_{ocv} + V_1) - R_0 I_{cell}) \quad 2$$

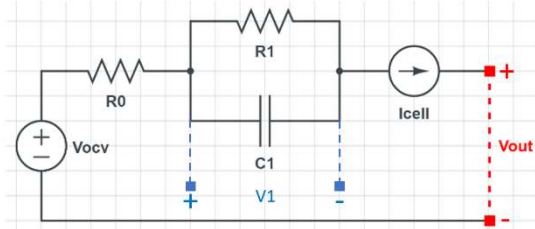
$$-R_0 I_{cell}^2 + (V_{ocv} + V_1) I_{cell} - P = 0 \quad 3$$

Letting $(V_{ocv} + V_1)$ be the equivalent voltage of the cell (V_{eq}), Equation 4 shows the solutions to the quadratic equation for cell current, the minimum solution is used for efficiency.

$$I_{cell} = \min\left(\frac{V_{eq} \pm \sqrt{V_{eq}^2 - 4R_0 P}}{2R_0}\right) \quad 4$$

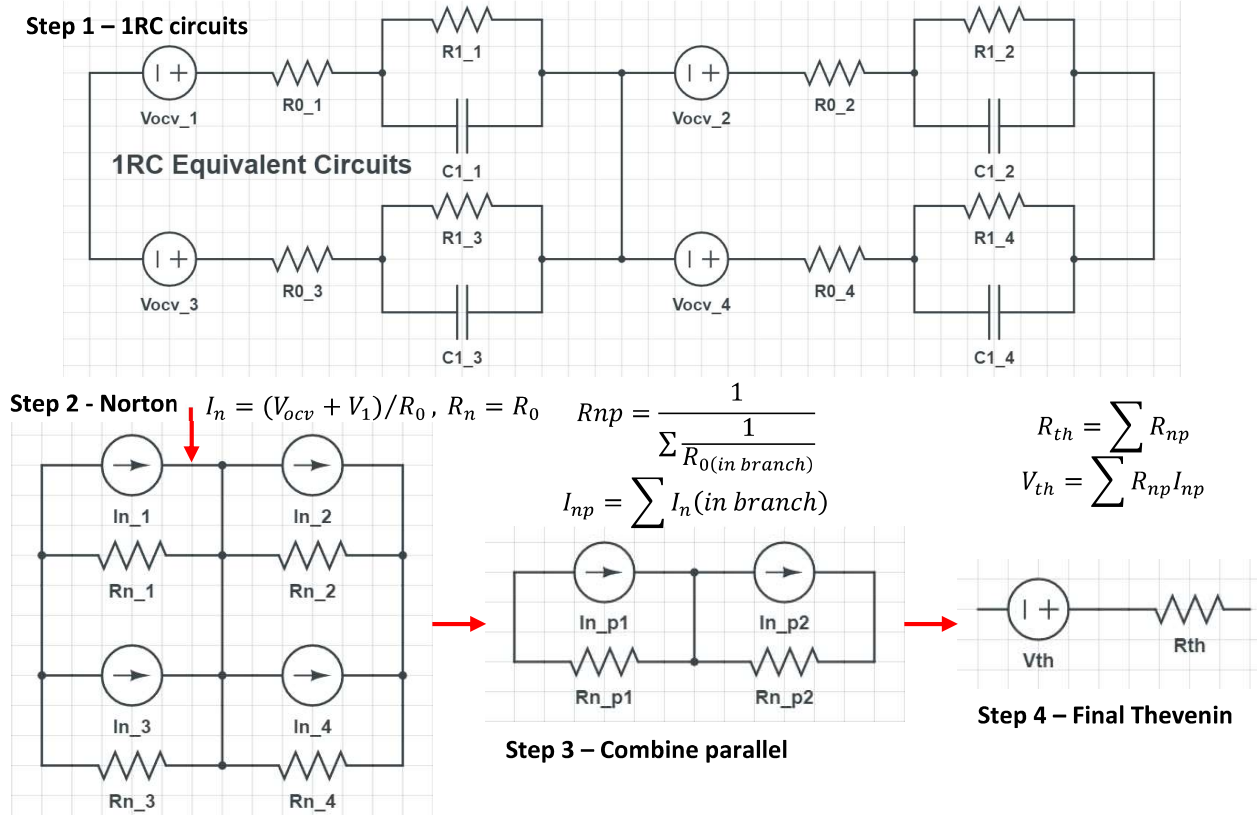
To calculate the full pack current, an equivalent voltage and resistance for the pack must be defined. This process has three steps, initially, all cells are converted into Norton equivalent circuits. The Norton current is the equivalent voltage divided by the ohmic resistance and the Norton resistance is the ohmic resistance of the cell. Next, the parallel cells are combined into s Norton equivalent circuits, where s is the number of cells in series, by summing the current sources and inverting the sum of the inverted resistances. Finally, the series cells are combined

Figure 4: Single RC equivalent circuit model



into a final Thevenin equivalent circuit. The Thevenin voltage is the sum of the resistances divided by the current in each cell and the Thevenin resistance is the sum of the resistances. This process is shown in Figure 6 for a two series, two parallel (2S2P) configuration and has been validated using Simscape with multiple different configurations. As modules are wired in series, this method works with multiple modules, the number of series cells is just increased.

Figure 5: Pack Thevenin equivalent circuit process



With a single parallel cell, the current in each cell is the pack current. However, when more parallel cells are added, the cell current becomes a combination of the load current and recirculating currents from voltage imbalances. As the number of parallel cells increases, calculating recirculating currents becomes more complex as all combinations of cells need to be accounted for. Meaning that for three cells in parallel, the current in the first cell will be dependent on the recirculation to the second and third cells.

Table 2 shows the increasing complexity of the current calculation as the number of parallel cells increases, where I_{pack} is the full pack current. This equation has been generalised; however, the notation is complex, so a written explanation is used. The denominator is the sum of all exclusive resistance combinations of length $p - 1$. The first term on the numerator is the voltage of the focused cell multiplied by the sum of the exclusive resistance combinations that do not contain the focused cell, of length $p - 2$. The middle numerator terms are the non-focused voltages multiplied by the product of all other resistances, excluding the focused and voltage cells, these terms account for recirculating currents. The final numerator term is the pack current multiplied by the product of all the resistances excluding the focused cell. This generalised form of the load equation has been validated with many parallel cells ($p < 8$) with Simscape. This method is consistent with any number of series cells, the process just needs to be completed separately for each set of parallel cells.

Table 2: Cell current calculation with increasing number of parallel cells

Parallel Cells	Cell 1 Current (I_{cell1})
1	I_{pack}
2	$\frac{V_1 - V_2 + I_{pack}R_2}{R_1 + R_2}$
3	$\frac{V_1(R_2 + R_3) - V_2R_2 - V_3R_2 + I_{pack}R_2R_3}{R_1R_2 + R_1R_3 + R_2R_3}$
4	$\frac{V_1(R_2R_3 + R_2R_4 + R_3R_4) - V_2R_3R_4 - V_3R_2R_4 - V_4R_2R_3 + I_{pack}R_2R_3R_4}{R_1R_2R_3 + R_1R_2R_4 + R_1R_3R_4 + R_2R_3R_4}$

5.2.3. State of charge

To determine SOC in the cells, the load current in each cell is normalised with the cell capacity and integrated. Equation 5 shows this process, where C_{cell} is the cell capacity. The multiplier is used to convert the charge from amp-seconds to hours. This is negative as the sign convention in this study considers positive current as discharge.

$$SOC = \int -\frac{1}{3600 C_{cell}} \frac{I_{cell}}{C_{cell}} dt \quad 5$$

5.3. Thermal model

5.3.1. Heat diffusion problem

Equations 6 and 7 are the heat diffusion equations for a single and multiple dimension case, where T is temperature, t is time, c_p is the mass based specific heat capacity, ρ is the density, k is the thermal conductivity and Q is the heat generation. In this model, the battery pack is considered thermally in three dimensions (x, y, z) so Equation 7 must be solved.

$$\frac{\partial T}{\partial t} c_p(x) \rho(x) = \frac{\partial}{\partial x} \left(k(x) \frac{\partial T}{\partial x} \right) + Q(x, t) \quad 6$$

$$\frac{\partial T}{\partial t} c_p \rho = \nabla \cdot (k \nabla T) + Q \quad 7$$

5.3.2. Finite volume model

The finite volume method involves splitting the body into many volumes and defining the thermal properties of each, including the thermal conductivity of each surface. Table 3 shows the parameters and their dimensions needed for the model, where n_x, n_y and n_z are the number of volumes in the x, y and z directions respectively.

Table 3: Finite volume model required parameters

Parameter	Dimensions		
	x	y	z
Boundary positions [m]	$n_x + 1$	$n_y + 1$	$n_z + 1$
Thermal conductivities [WK^{-1}]	$n_x + 1, n_y, n_z$	$n_x, n_y + 1, n_z$	$n_x, n_y, n_z + 1$
Mass [kg]	n_x, n_y, n_z		
Heat capacity [$Jkg^{-1}K^{-1}$]	n_x, n_y, n_z		

Additionally, boundary conditions need to be defined. [39] describes the three main types of boundary condition for this method. Prescribed temperature or Dirichlet boundary conditions represent a fixed temperature at the boundary, governing the heat flux in/out of the

*Automotive Engineering MEng; B723936; Project supervisor: Dr Thomas Steffen

body. Prescribed heat flux or Neumann conditions define a fixed heat flux in/out of the body. Finally, Robins conditions use Newton's law of cooling to provide a more complex boundary condition usually reserved for flowing fluids at the boundary. Functionality for Dirichlet and a form of Neumann boundary condition known as an insulated boundary condition have been added. In this study insulated boundary conditions are used, helping to isolate the performance of the pack. Equation 8 shows the insulated boundary conditions in the x direction, where L_x is the length of the pack in the x direction.

$$k(0) \frac{\partial T}{\partial x}(0, t) = k(L_x) \frac{\partial T}{\partial x}(L_x, t) = 0 \quad 8$$

To solve the second order partial differential equation the differentials will be computed separately in each direction and combined with cell heat generation and heat flux from coolant flow. As shown in Equation 7, the first differential is the change in temperature in each direction. This is then multiplied by the thermal conductivities to get the heat flux at each boundary. Temperature boundary condition values are used for the temperature differential calculation, however, as insulated conditions are in use the temperature values are arbitrary. To match the dimensions of the temperature and thermal conductivity matrices for the multiplication of the differential, the boundary conditions are added to the temperature matrices separately. Table 4 shows how the temperature differences are calculated using a simple vector case with five volumes in one dimension.

Table 4: Temperature difference calculation example

Temperature vector	5	4	3	2	1
Add start boundary	0	5	4	3	2
Add end boundary	5	4	3	2	1
Calculate temperature difference	-5	1	1	1	1
Positive difference indicates heat flow to the right					

After multiplying the above temperature difference by the thermal conductivity to get the heat flux at each boundary, a similar process is completed for the second differential. This differential is used to find the difference between the boundary heat flux in and out of each volume, resulting in the overall volume heat flux. Table 5 continues the example, showing the second differential and heat addition, leading to the net volume flux.

Table 5: Net volume flux calculation example

Temperature difference	-5	1	1	1	1	1
Thermal conductivity	0	1	1	1	1	0
Boundary flux	0	1	1	1	1	0
Volume flux	-1	0	0	0	0	1
Heat generation + Coolant flux	1	2	3	4	5	
Net volume flux	0	2	3	4	6	
Positive volume flux heat gain						

Using this, the temperature change can be calculated by dividing the flux by the product of the specific heat capacity and mass of each volume. This is then integrated for the temperature.

5.3.3. Heat generation

Cell heat generation (Q_{cell}) is being considered as purely ohmic, this is calculated using the heat dissipation by the resistors in the ECM. Equation 9 shows this, where n is the total number of resistors (2), I_i is the current in the resistor and R_i is the resistance.

$$Q_{\text{cell}} = \sum_{i=1}^n I_i^2 R_i \quad 9$$

The heat generation is considered as a volume averaged heat source. The validity of this assumption is dependent on the layout of the cell. If both the positive and negative tabs are positioned on one side of the cell it is more likely that heat generation will be concentrated on one side. However, in this case, the example cell used in the e-tron pack has one tab on each side of the cell, so it is more likely that the distribution of heat generation is uniform, further supporting this assumption.

5.3.4. Materials dictionary

An expandable materials dictionary spreadsheet containing all the material parameters needed to initialise the thermal model has been produced. In the initialisation the volume materials are specified with the material ID. Table 6 shows the current materials dictionary, at this point only three materials are in the model, the cell material, aluminium, and coolant.

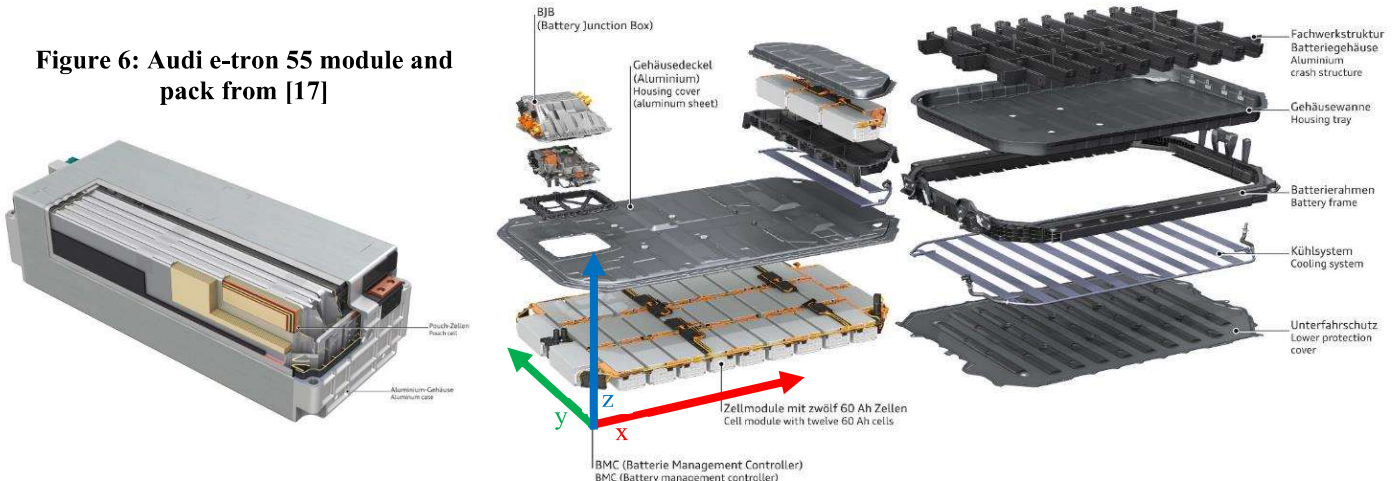
Table 6: Materials dictionary

ID	Name	Specific heat capacity [Jkg ⁻¹ K ⁻¹]	Density [kgm ⁻³]	In-plane thermal conductivity [Wm ⁻¹ K ⁻¹]	Cross-plane thermal conductivity [Wm ⁻¹ K ⁻¹]
1	Cell	1100 [18][19][11][20]	1506 [37]	26.5 [21]	0.878 [21]
2	Aluminium	870 [40]	2712 [14]	236 [15]	236 [15]
3	50/50 Ethylene Glycol	830 [16]	1079 [16]	0.258 [16]	0.258 [16]

5.3.5. Pack layout simplification

The pack layout used in this model is based on the 2021 Audi e-tron 55 quattro. The left of Figure 7 shows a module layout from [17] as well as the sign convention used in this model, it contains 12 LG Chem cells stacked in the thickness direction. It is also clear from the image that the module walls on the ends are thicker than the sides. There is complex geometry in the module design with a variety of materials, to simplify this, the module is modelled as a stack of cells in a pure aluminium box.

Figure 6: Audi e-tron 55 module and pack from [17]



To determine the thickness of the aluminium walls, the approximate mass of the module was used (13kg [17]). As well as this it was assumed that the end walls were twice as thick as the side walls. Equations 10, 11 and 12 show how the volume of aluminium in the module can

be calculated based on the wall thickness, where x is the thin wall thickness and w , l and t are the cell width, length, and thickness respectively.

$$V_{total} = (2x + w)(2x + 12t)(4x + l) \quad 10$$

$$V_{cell} = 12wtl \quad 11$$

$$V_{al} = V_{total} - V_{cell} = 16x^3 + (4l + 96t + 8w)x^2 + (24lt + 2lw + 48wt)x \quad 12$$

A target aluminium volume was found using the remaining mass for the module after the 12 cells are considered, Equation 13 shows this. Where M_{mod} is the module mass ($13kg$), M_{cell} is the cell mass ($0.82kg$ [17]), and ρ_{al} is the aluminium density ($2712kgm^{-3}$ [14]).

$$V_{target} = \frac{M_{mod} - 12 * M_{cell}}{\rho_{al}} = 1165cm^3 \quad 13$$

Using this target, the cubic equation was solved to get an x value of $4mm$. This results in a module mass of $12.996kg$, very close to the target.

The right of Figure 7 shows the pack layout from [17], it has 36 modules, for a total of 432 cells. The modules are arranged in a grid, separated with an aluminium crash structure. The pack is surrounded by a frame and upper and lower covers. This model is only considering a uniform skateboard type pack layout with a single layer. Therefore, the second layer, as well as the front and back modules are not considered, resulting in a reduced pack of 27 modules, hence the use of the $71kWh$ vehicle parameters for power requirements.

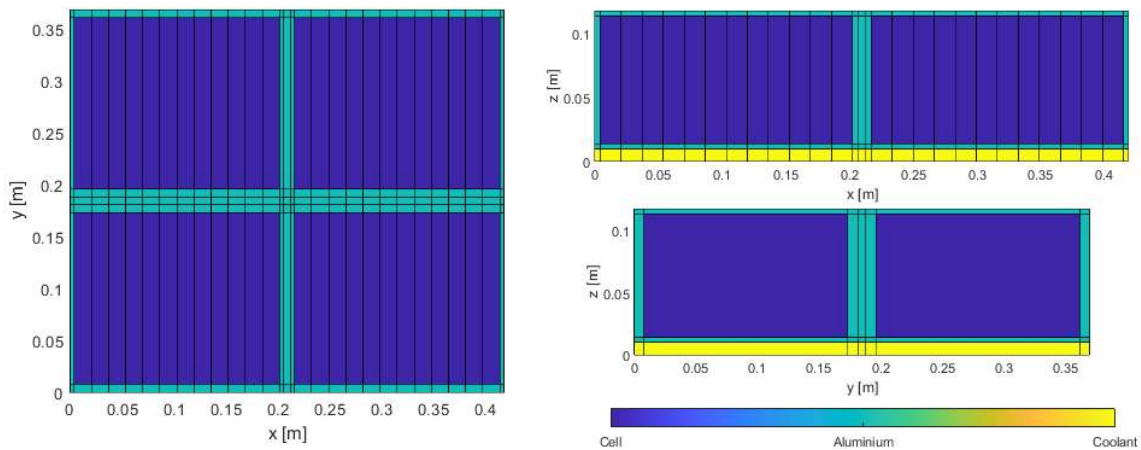
As the battery pack is being considered as insulated, modelling of the outer structures is omitted. This includes the protection covers, housing tray, and outer battery frame. Also, the battery junction box is not modelled. The insulated assumption is reasonable as current battery design has an emphasis on protecting the battery from extreme environmental temperatures [41]. Additionally, it is beneficial to isolate the battery from the environment to allow efficient heat storage during warm up stages in cold conditions, this means the battery will not need to be reheated after short idle stages. If this was not the case in a specific study, boundary conditions could be altered to simulate heat transfer to/from a roughly ambient temperature frame and chassis.

The crash structure is positioned between modules and will likely facilitate heat transfer between modules, because of this it is included in the model. From [17], it is known that the crash structure is made of aluminium. As no thickness is provided an estimation of $5mm$ was initially used for the crash structure. However, this resulted in volumes with very low thermal inertia, leading to instability errors in the solution. This was resolved by increasing the thickness to $6.5mm$ increasing the thermal inertia of the small elements.

As expected, the final mass of the model is significantly lower than the advertised pack mass of $580kg$ [37] at $374kg$ (excluding coolant). A large majority of the additional mass will be accounted for with the frame and housing that has been discounted in this case. However, some of the additional mass will be due to the wiring, which could potentially alter the thermal performance of the modules. As this model is not aimed to accurately represent the exact e-tron pack, the potential difference in thermal inertia is not an issue in this study. In future work if the base model produced here was to be used to complete accurate tests for a specific pack parameterisation will be beneficial.

Figure 8 shows the simplified pack structure, modelling the cells as a single volume for clarity. In simulations multiple volumes are used to evaluate temperature gradients over the cells. To show the base structure, a reduced size pack is shown with 4 and 2 modules in the x and y directions compared to 9 and 3 in the full pack. In the full pack the layout is simply replicated for the additional modules. Also, the cell length has been halved to better show the crash structure geometry. This includes bottom cooling, where the coolant is assumed to be a flat plate coolant covering the bottom of the pack (see Section 5.4.2).

*Automotive Engineering MEng; B723936; Project supervisor: Dr Thomas Steffen

Figure 7: Reduced pack structure and materials

5.3.6. Boundary thermal conductivities

For model configuration the thermal conductivity at each volume boundary must be defined. Heat transfer at a boundary is a combination of conduction, convection, and radiation. It is assumed that convection is sufficiently small in this situation to be ignored.

For boundaries between two volumes of a single solid material, the heat transfer can be calculated using pure conduction. Thermal conductivities of neighbouring volumes are averaged to find the boundary conductivity. To determine the thermal conductivity of the individual volumes, the length in the direction of the heat flow (L) and area perpendicular to the heat flow (A) will be used. Equation 14 shows this calculation, where k_{mat} and k_{vol} are the thermal conductivities of the material and volume respectively.

$$k_{vol} = \frac{k_{mat}A}{L} \quad 14$$

Alternatively, heat transfer at the boundaries between different materials or objects will be a combination of conduction and radiation (convection discounted) based on the interface material and other factors such as contact pressure. In general, the highest thermal conductivity comes from conduction through an interface material, this is a function of the interface material thermal conductivity and thickness. The smallest possible value will be pure radiation, with no physical contact between the materials.

Two interface materials for boundary conductivity have been considered in this model. Firstly, for heat transfer between cells and from cells to the module walls, the pouch cell film casing is considered as the interface. The pouch thermal properties from [42] are used for this: thermal conductivity is $0.269 Wm^{-1} K^{-1}$ and the thickness is $0.254 mm$, this thickness will be double for cell-cell connections as two layers of film are present. Secondly, heat transfer from the module to coolant channels will use a thermal gel as [17] states that this method is used in the pack construction. This will also be considered for heat transfer between modules and the crash structure. Henkel produce thermal gels for the automotive industry [43], they offer a thermal gel with conductivity of $3.5 Wm^{-1} K^{-1}$ for use over a range of gap sizes from 0.5 to $3 mm$ [44]. A mid-range thickness value of $1.5 mm$ will be used in this model. Equation 14 is used to calculate the interface material conductivity at the relevant boundaries.

Lithium-ion packs operate with small temperature differences so linearised radiation can be used with a small error. To linearise radiation, the thermal conductivity between two $1m^2$ faces was calculated at various temperature combinations using black-body radiation to find a mean thermal conductivity per unit area of $5.4268 WK^{-1} m^{-2}$. This process is shown on the left of Figure 9. The right of Figure 9 shows the effectiveness of the assumption, with a maximum error of 5% with a $10^\circ C$ difference. This is a reasonable error for the simplicity of the

*Automotive Engineering MEng; B723936; Project supervisor: Dr Thomas Steffen

implementation, in future work a more complex radiation method could be implemented if required, including the emissivity of each face. As radiation is directly proportional to area, the unit thermal conductivity above can be multiplied by the boundary area for the boundary thermal conductivity in the model.

Figure 8: Radiation linearisation results for a 1m² contact area – maximum error of 5%

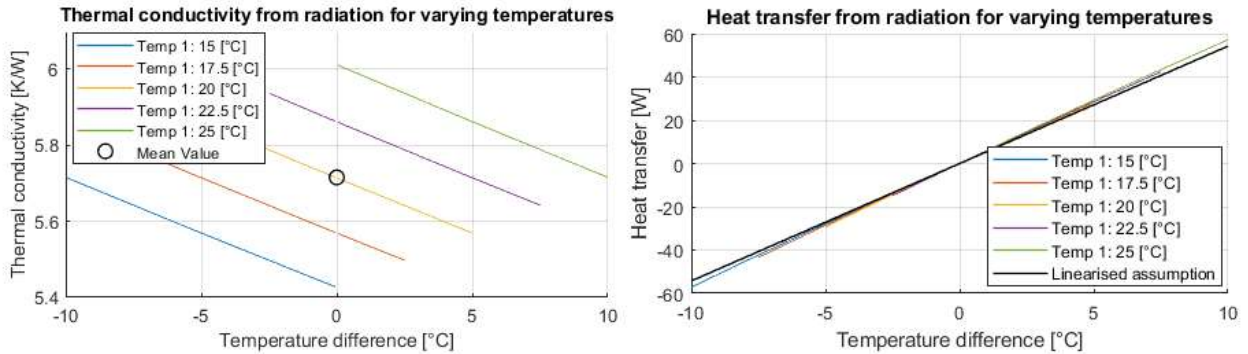


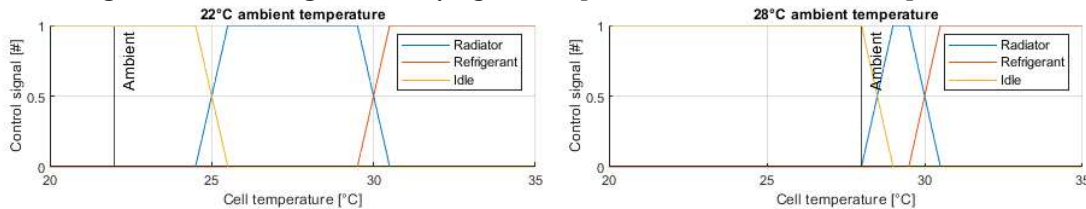
Figure 7 shows that the connection between cells and the module walls varies with the dimension of the cell. As an initial assumption in this work, heat transfer in the width and thickness directions uses the max value from the pouch conductivity as the connection appears to be substantial. However, in the length direction, due to the large air gaps pure radiation is assumed. For parameterisation of this model for a specific pack the tuning of these parameters will be key, shown by the sensitivity analysis in Section 7. Additionally, if testing the long-term performance of a pack, these parameters will likely change with degradation. As cells degrade, they produce gases, these accumulate at the edges of the pouches, resulting in an increased dependence on radiation for heat transfer from the active material to the pouch. Also, heat transfer from module walls to the crash structure will be assumed as pure radiation. The physical connection between the crash structure and modules is likely to be limited to allow the crash structure to be deformed without loading the modules.

5.4. Control and thermal management

5.4.1. Control

For representative model performance during drive cycles some control is needed to vary the cooling method based on the pack temperature. A basic control method has been implemented to distribute coolant flow between a radiator, refrigerant loop, and bypass (idle). The control uses the max cell temperature to reduce the likelihood of a single cell exceeding target temperature ranges. Figure 10 shows the transition from idle to passive and active cooling as the pack temperature increases past the target value of 25°C for two different ambient temperatures. The radiator will only be used for cooling if the pack temperature is above the ambient temperature. To calculate pack input coolant temperature, coolant flow is split, and individual flow temperatures are recombined based on the flow weighting.

Figure 9: Control signals at varying cell temperature at two ambient temperatures



5.4.2. Thermal management

Figure 11 shows the e-tron thermal management system in more detail from [17]. The pack is cooled from below using aluminium extrusions bonded to the modules with thermal gel. These extrusions contain multiple small channels to increase the surface area with coolant. The image also shows a refrigerant circuit responsible for cooling the heated coolant, additionally this could heat the coolant in cold conditions, however, in this study only cooling is considered.

To adequately model the thermal management system, key global effects need to be modelled. The most notable effects are the temperature gradient in the direction of the coolant flow and the reduction in coolant temperature from the refrigerant loop and/or radiator. To facilitate these effects in the model without excess complexity several assumptions will be made.

5.4.2.1. Coolant and heat sink

The coolant used in this model is a 50/50 ethylene glycol/water mixture as used in [45], this is a common coolant at varying proportions in the automotive industry.

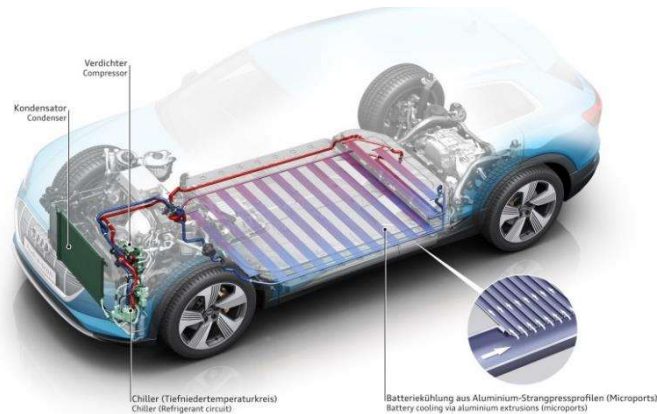
Heat transfer from the aluminium extrude will primarily be forced convection, to consider this in detail a function would need to be formed to determine heat transfer with respect to the heat sink geometry and coolant flow rate. This would involve calculating the Nusselt number for the heat sink. To greatly simplify this mechanism, it has been assumed that the heat sink is sufficiently designed for the heat transfer to the coolant to be limited by the transfer from the module casing to the extrude via the thermal gel. Due to this assumption, the coolant and aluminium heat sink can be lumped together. Finally, although the e-tron example uses separate extrudes for the module rows, this model will use a simplified single plate cooling approach. The result is a 10mm thick layer of coolant on the full bottom surface of the pack, shown in Figure 8. The parameterisation of the coolant thickness and heat transfer will be key for modelling specific systems in future work.

Basic conductive heat transfer as discussed before will be modelled in the coolant. As well as this, the heat transfer due to coolant flow needs to be calculated to produce the desired temperature gradients. First the temperature differential in the coolant is calculated using the inlet temperature. This process varies based on the flow direction, if the flow is positive/negative, the inlet temperature is added to the start/end of the temperature vector. After this, the temperature on the opposite side of the inlet is removed and the difference is calculated with the original temperature vector. An example of this calculation for positive flow is shown in Table 7. For negative flows the sign of the temperature difference is flipped.

Table 7: Coolant temperature difference calculation example

Temperature vector	1	2	3	4	5
Add inlet temperature (1)	1	1	2	3	4
Remove outlet temperature (5)	0	1	2	3	4
Calculate temperature difference	0	-1	-1	-1	-1
Positive difference indicates heat flow into the volume					

Figure 10: Audi e-tron battery pack cooling from [17]



The temperature difference is then multiplied by the coolant specific heat capacity and mass flow rate to produce the heat flow into each coolant volume due to the upstream coolant. The heat flow values due to the coolant flow will then be added to the cell heat generation to produce the net heat gain for the model.

Finally, an appropriate coolant flow rate needs to be defined for the model. To remove the non-linear contributions of varying flow rates for the model order reduction, a constant flow rate will be used in this study. If required, a varied flow rate could easily be implemented in future work, however, the order reduction method may need to be revisited. [45] uses two identical coolant pumps to cool a $24kWh$ battery, motor, power electronics, and cabin in a vehicle emulation rig. A single coolant pump flow rate ranges from $0.14 - 0.25kgs^{-1}$ in this study. Assuming one of these pumps would be equivalent to cooling the battery and scaling the pump flow rate based on pack energy results in a reasonable target range of $0.42 - 0.75kgs^{-1}$ for this pack. Additionally, it is critical for the solution that the mass of coolant flow through a volume in a single time step does not exceed the mass of the volume. For the full pack with a $0.1s$ time step this limit value is $1.34kgs^{-1}$. To allow the flow rate to scale with pack size, the flow in the pack will be defined based on the maximum value. The constant flow rate is defined as the $0.5\dot{m}_{max}$, where \dot{m}_{max} is the maximum flow rate for a stable solution. This is $0.67kgs^{-1}$ for the $71kWh$ pack, comfortably within the reasonable range shown above.

Pack output temperature is determined using a weighted average of the output side coolant temperatures based on the flow through each volume.

5.4.2.2. Heat rejection

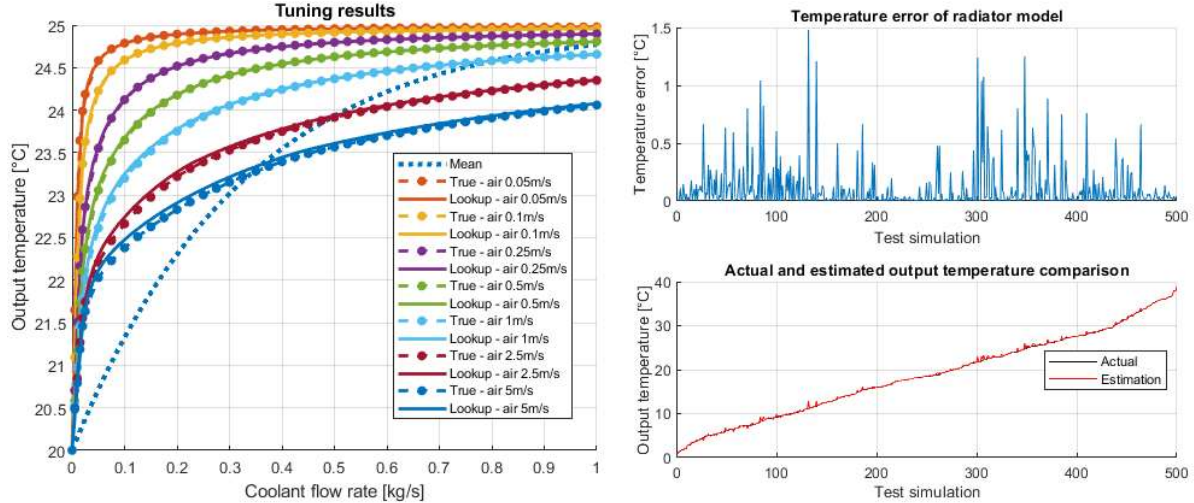
It is common for battery thermal management systems to operate with passive or active cooling based on the conditions. Passive cooling uses the ambient air to cool coolant using a radiator, whereas active cooling uses a compressor and expansion valve to cool coolant with sub ambient temperature refrigerant. To implement both modes into the model, a radiator and refrigerant loop model were parameterised.

Simple radiator functionality can be modelled as an exponential equation, as coolant flow (\dot{m}) increases, the output temperature (T_{out}) exponentially tends from ambient temperature (T_{amb}) to the input temperature (T_{in}). The decay rate is defined with a nominal flow (\dot{m}_{nom}). Equation 15 shows the radiator exponential approximation.

$$T_{out} = T_{amb} + (T_{in} - T_{amb}) * \left(1 - e^{-\frac{\dot{m}}{\dot{m}_{nom}}}\right) \quad 15$$

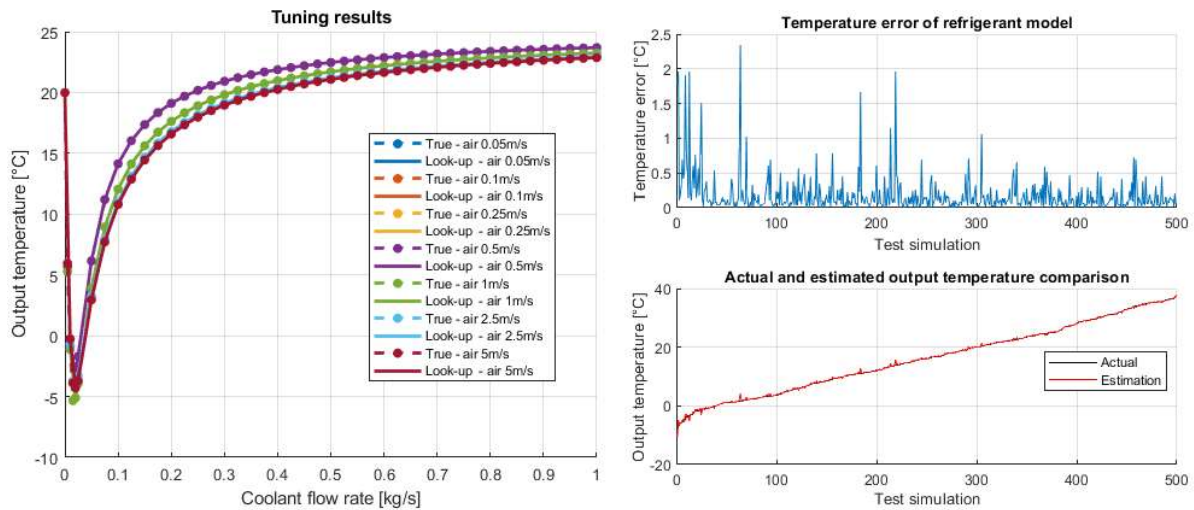
The nominal flow was parameterised using a Simscape based radiator model from [25], it is modelled as a liquid to air heat exchanger with unmixed fluids using the effectiveness number of transfer units (e-NTU) method shown by equations 2-5 in [25]. The Dittus-Boelter equation is used to calculate the Nusselt number of the heat exchanger and correction factors for the air and liquid sides were applied to fit the data from [46]. This heat exchanger was placed in a basic Simscape model using controlled reservoirs and flow rate sources. To fit the nominal flow over a range of conditions, coolant input temperature, coolant flow rate and air velocities were varied, and the best fit value was determined at each of these points. Initially, a mean value was used, however, this was inaccurate across a wide temperature range. Instead, a 2D look-up table of nominal flow values is used with coolant flow and air velocity break points, using a mean value for each point over the range of input temperatures. The left of Figure 12 shows the results of the tune for a variation of air speeds and the right shows a 500-simulation validation from a wider range of random inputs. The mean and maximum output temperature error were $0.10^\circ C$ and $1.47^\circ C$ respectively, these errors are low enough to implement a good representation of heat rejection in the system.

*Automotive Engineering MEng; B723936; Project supervisor: Dr Thomas Steffen

Figure 11: Radiator look-up table tuning and wider validation results

A similar Simscape model was produced to implement active cooling into the model using the parameters from the example electric vehicle thermal management model from Mathworks [47] and R123yf refrigerant. The refrigerant loop was modelled with a compressor, expansion valve, refrigerant to coolant heat exchanger (chiller) and refrigerant to air heat exchanger (condenser). These parameters are also used in [25], the heat exchangers are modelled in a similar way to the radiator, using the e-NTU method described by the same equations in [25]. A constant maximum compressor load was assumed for the parametrisation. Also, a minimum 0.5ms^{-1} saturation block was added to the air velocity to avoid maximum pressure exceptions in the refrigerant caused by the lack of heat rejection from the system.

To model the refrigerant loops without excess complexity a pure look-up table approach was used to parameterise the loop using an additional dimension for input temperature. The same method as above was used to produce a 3D look-up table for output temperature with coolant flow, air velocity and input temperature breakpoints. Figure 13 shows the results of the tuning process, the left graph shows some of the tuning data and the right shows the results of wider validation. The mean and maximum output temperature errors were 0.18 and 2.34°C respectively, although these errors are higher than the radiator, due to the increase in complexity they have been considered as low enough for the simplicity of the implementation.

Figure 12: Refrigerant look-up table tuning and wider validation results

5.5. User configuration

5.5.1. Input retrieval

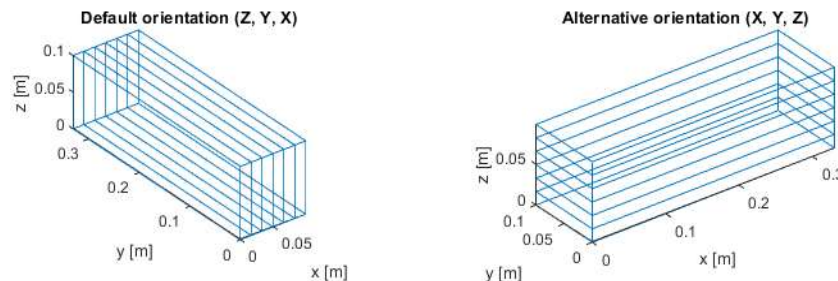
A key aim in the project was for the model to be configurable. For this, three sets of inputs are collected on initialisation using input dialog boxes. These are shown in Figure 14.

From left to right, the first shows the base pack layout inputs, it specifies the number of cells and modules, how many regions are used to thermally model the cells as well as the orientation of the modules. Additionally, whether the crash structure is modelled, or modules are touching directly. Figure 15 shows two examples of how the cell orientation effects the layout of the pack, the figure shows a single stack of cells, these stacks will then be arranged based on the number of modules in each direction.

Figure 13: User configuration input dialog boxes

Base pack layout		Thermal config	
Cells per module	Series cells - per module [#]	Ambient Temperature [°C]	-
4	25	y start boundary [°C]	nan
Parallel cells - per module [#]	Cooling	y end boundary [°C]	nan
3	Use unlisted input for no cooling e.g. none or no z start boundary [°C]	z start boundary [°C]	nan
Modules in pack x and y direction	Top cooling? [+/-xy]	z end boundary [°C]	nan
Module count x [#]	none	z end boundary [°C]	nan
9	Bottom cooling? [+/-xy]	z end boundary [°C]	nan
Module count y [#]	+y	z end boundary [°C]	nan
Cells regions for FVM in cell directions	Boundary conductivities	Cycle selection [#]	-
Cell regions length [#]	0 min - 1 max	1 L_NEDC	-
5	Cell-cell [#]	2 L_NEDC_AB	-
Cell regions width [#]	1	3 L_NEDC_H	-
3	Cell length-module [#]	4 L_NEDC_REV	-
Cell regions thickness [#]	0	5 WLTC_1	-
1	Cell width-module [#]	6 WLTC_2	-
Orientation of cells/modules in pack	1	7 WLTC_3	-
Cell length dimension [x,y,z]	Cell thickness-module [#]	8 Zero vel	-
y	1	Cell width-module [#]	7
Cell width dimension [x,y,z]	Module-crash struct/module [#]	Simulation options	-
z	0	Cycle count [#]	1
Include crash structure [y/n]	Init temperature bias [°C]	Model time step - high values lead to errors [s]	-
y	0	0.1	-
		Logging sample time multiple - rounded up [#]	-
		10	-

Figure 14: Cell orientation default and alternative example (length, width, thickness)



The second set of inputs shows the main thermal configuration, including ambient and initial temperature, cooling, and the boundary conductivities. Temperature bias is the difference between the initial pack temperature and the environment, for example pack temperature could start at 30°C with 20°C ambient to simulate performance after a fast charge. Although the base pack uses bottom cooling, top cooling has been added using the same assumptions. Both can be used simultaneously, for this the flow is split between the top and bottom.

As discussed in Section 5.3.6, theoretical minimum and maximum values have been defined for the heat transfer at different boundaries, the boundary conductivities allow a number between 0 and 1 where 0 is the minimum value and 1 is the maximum, values in-between use linear interpolation for the conductivity.

Finally, the boundaries and simulation preferences are defined. This allows the use of insulation boundaries, as used in this study, or temperature boundaries. The drive cycle is defined from a finite list of options, including a zero-velocity cycle, useful for testing the cooling capabilities without heat generation. The cycle count allows repeated or partial cycle simulations. In future work, additional cycles can be added simply with a two-column velocity and time matrix. The time step and logging sample times can also be altered based on the requirements of the simulation and computer specifications.

5.5.2. Model implementation

Due to the large amount of variation in the model it is important that all methods are implemented in a robust way, allowing for all current functionality as well as simple implementation of additional features in future work. The model has been produced in a way that separates the initialisation from the model, this means that if the relevant parameters are provided, including electrical layout, thermal layout (boundaries etc.) and the mapping indices (see below), the overall pack layout can be completely changed without issue.

Implementing the thermal and electrical models independently is somewhat simple, however, a key aspect of the full model is the mapping between the thermal and electrical models. Using the inputs, matrices containing indices are defined for mapping during the initialisation using multiple loops. The initial process for this is complex but during runtime only simple indexing and reshaping is required, reducing computation time. Figure 16 overviews the outcome of this process, showing the index assigned to each volume in an xy plane layer of a reduced size pack. Cells in a parallel branch are stacked on top of each-other as done in the e-tron modules [17]. Shown in the circuit layout in Figure 6, cell number increases along each series chain so the cell ID for a stack of parallel cells will increase based on the number of series cells (1,17,33 for the first branch of 4S3P and 4module). As all modules are wired in series, sharing the same current, the order modules are considered in this step is irrelevant to the solution.

Mapping cell heat generation to volumes is completed fully with inbuilt Simulink blocks as shown in Figure 17. The mapped cell heat values are divided equally between the cell volumes as uniform heat generation is assumed.

Figure 15: Cell positioning for a reduced 4S3P pack in the xy plane

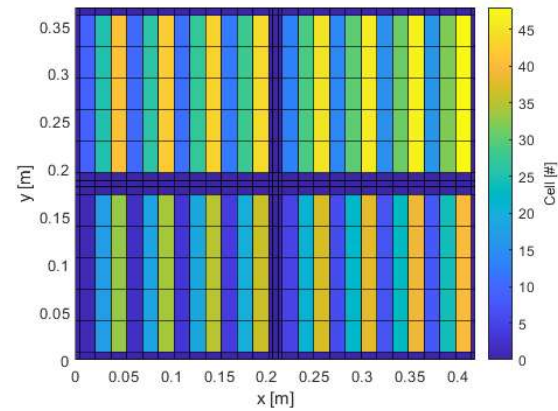
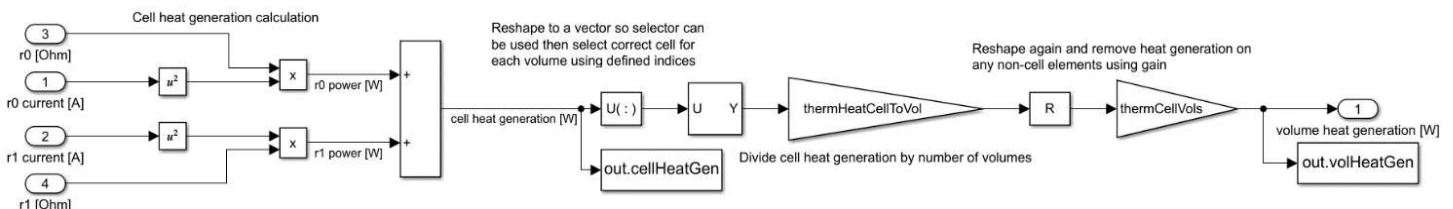


Figure 16: Cell heat generation calculation and mapping to volume heat generation



Alternatively, mapping from the volume temperatures to cell temperatures is more complex as the mean of each set of volumes is required for the cell temperature. This resulted in simpler implementation with a Matlab function block. When possible, inbuilt Simulink blocks are used for model speed, however, from the Simulink profiler, the maximum speed improvement for the model would be $\sim 1\%$ if using inbuilt blocks here, a negligible increase.

A similar process is completed to generalise the complex electrical loading equation, index matrices are defined, and a Matlab function block is used to determine the loading. This has a larger contribution to overall simulation time so Simulink blocks could be used in future work to improve the computation time.

Another key area is flow division, in the initialisation the proportion of flow in volumes in each direction is calculated based on cross-sectional area. Positive and negative flow in each direction is then considered separately in the model and fluxes are recombined. This method allows coolant flow at any point in the model, allowing testing of alternative cooling methods such as coolant flow between modules. This method also easily handles changing directions of flow, allowing study of the effects of periodic flow direction changes on degradation.

6. Order reduction

6.1. Reduced order model implementation

To implement a principal component analysis (PCA) based reduced order model the inbuilt Matlab PCA function [35] was used. The input to this function is a matrix of size $n \times m$ where m is the number of data points and n is the number of values recorded for each data point. To retrieve this data a simulation of five WLTC cycles was completed for the base pack layout at an ambient temperature of 25°C , logging data once per second. After some experimentation, 25°C produced the best PCA results for passive cooling, however there were issues for active cooling, shown in Section 6.2. The base layout has 18492 volumes/data points and the simulation time was 9005s leading to an input matrix size of 9005×18492 . The function has the following outputs, *coeff*, *score*, *latent*, *tsquared*, *explained* and *mu*. In this work only *coeff* and *score* are used. *coeff* contains the principal component coefficients with a column for each component and rows for each data point. *score* contains the score for each principal component over the time steps. The product of *coeff* and *score* is the centred original data. For this process 10 principal components have been used, in future work an additional investigation into the effects of changing this number could be beneficial.

For a Simulink implementation, the PCA results were converted into a linear state space model. The base equation for this is shown in Equation 16, where A is the constant state matrix, B is the constant input matrix and x and \dot{x} are the states and state time derivative respectively.

$$\dot{x} = Ax + Bu \quad 16$$

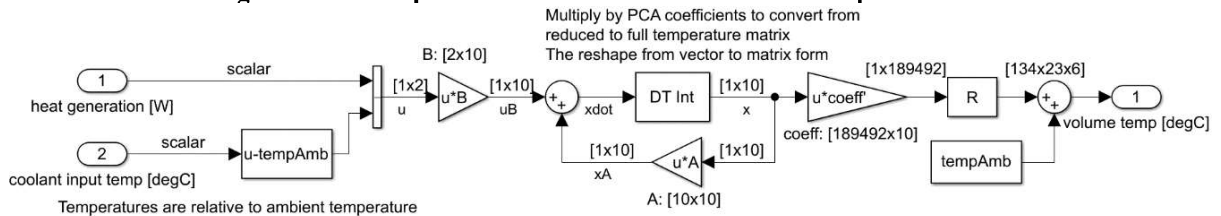
The states are the principal components from the original data. The selected inputs for the thermal model were the heat generation and coolant input temperatures. To keep the number of inputs low, the total heat generation was used rather than the individual cell heat generations, heavily simplifying the electrical side of the model. Additionally, as centred data is used in the next step, coolant temperature is measured relative to the equilibrium, in this case the ambient temperature. Linear regression was used to find A and B , this involves a left-hand divide of a stacked matrix containing the *score* and u by the reduced state time derivative (\dot{x}_r), this is shown in Equations 17 and 18. Here u is a 9005×2 matrix containing the total heat generation and relative coolant input temperature for each time step. \dot{x} is calculated using the centred original data, the data is centred by subtracting the mean value of each data point from the data.

$$\dot{x}_r = \dot{x} \cdot \text{coeff} \quad 17$$

$$\begin{bmatrix} A \\ B \end{bmatrix} = [\text{score} \quad u] \backslash \dot{x}_r \quad 18$$

Figure 18 shows the Simulink implementation of the reduced order state space model with the dimensions of each signal. Equation 16 is solved using a discrete time integrator and then the reduced form is converted into the full form using the principal component coefficients. As stated above, the environmental temperature is considered as equilibrium hence the use of ambient temperate addition and subtraction. To maintain the original 3D matrix format in the thermal model a reshape block is used to convert the volume temperatures from a 1D vector to the original form.

Figure 17: State space reduced order model Simulink implementation



*Automotive Engineering MEng; B723936; Project supervisor: Dr Thomas Steffen

6.2. Order reduction results

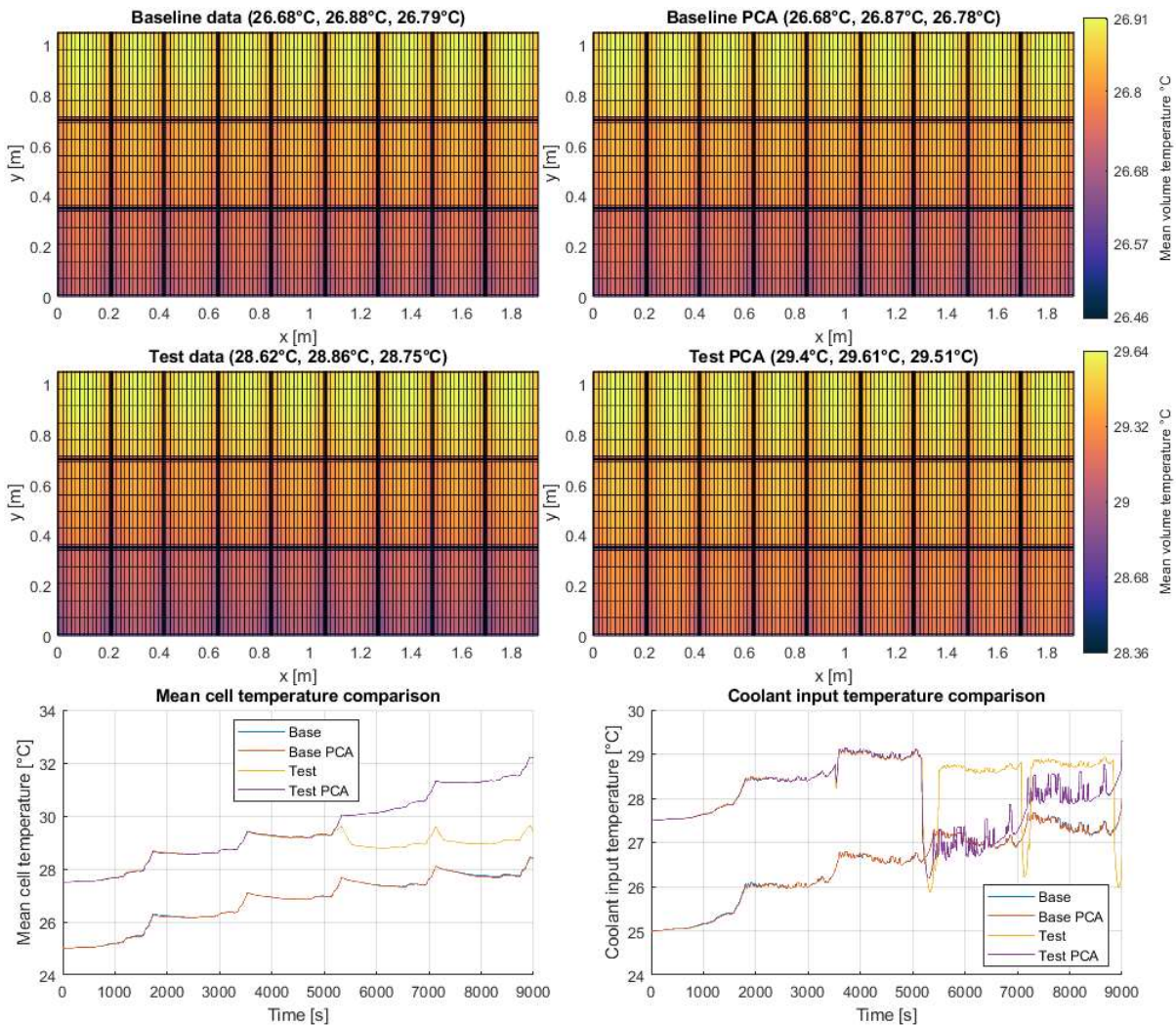
Due to its simplicity, the state space model runtime reduced to 53.3s from 262.8s, an 80% decrease. The electrical model was also unchanged, reducing the electrical model to a single average cell would further reduce model time and produce very similar results.

Figure 19 shows the order reduction results, including slices of the mean volume temperatures and comparisons of the mean cell and input coolant temperatures. Accuracy of the PCA assumption at the baseline simulation was very good, mean, minimum, and maximum cell temperatures were all within 0.01°C after the full cycle and temperature gradients are indistinguishable. Additionally, high transient accuracy is shown in the bottom figures.

However, the original PCA produced in the ambient cooling region of the pack was not effective at modelling active cooling. This is shown by the steep drop in accuracy at the switching point from passive to active cooling at 29.5°C in the test simulation. The PCA was repeated with simulations of the same length at other ambient temperatures with a combination of active and passive cooling, however this simply resulted in poor accuracy for both the active and passive cooling modes, hence the decision to maintain the 25°C base point.

Despite this, the initial results are promising, in future work the problem could be negated with a more robust PCA derivation process with more data points over a wider range of environmental temperatures. Additionally, if this fails, two different PCA's could be switched between based on the cooling method.

Figure 18: Model order reduction results, baseline at 25°C and test at 27.5°C , (min, max, mean cell temperature)



7. Sensitivity analysis

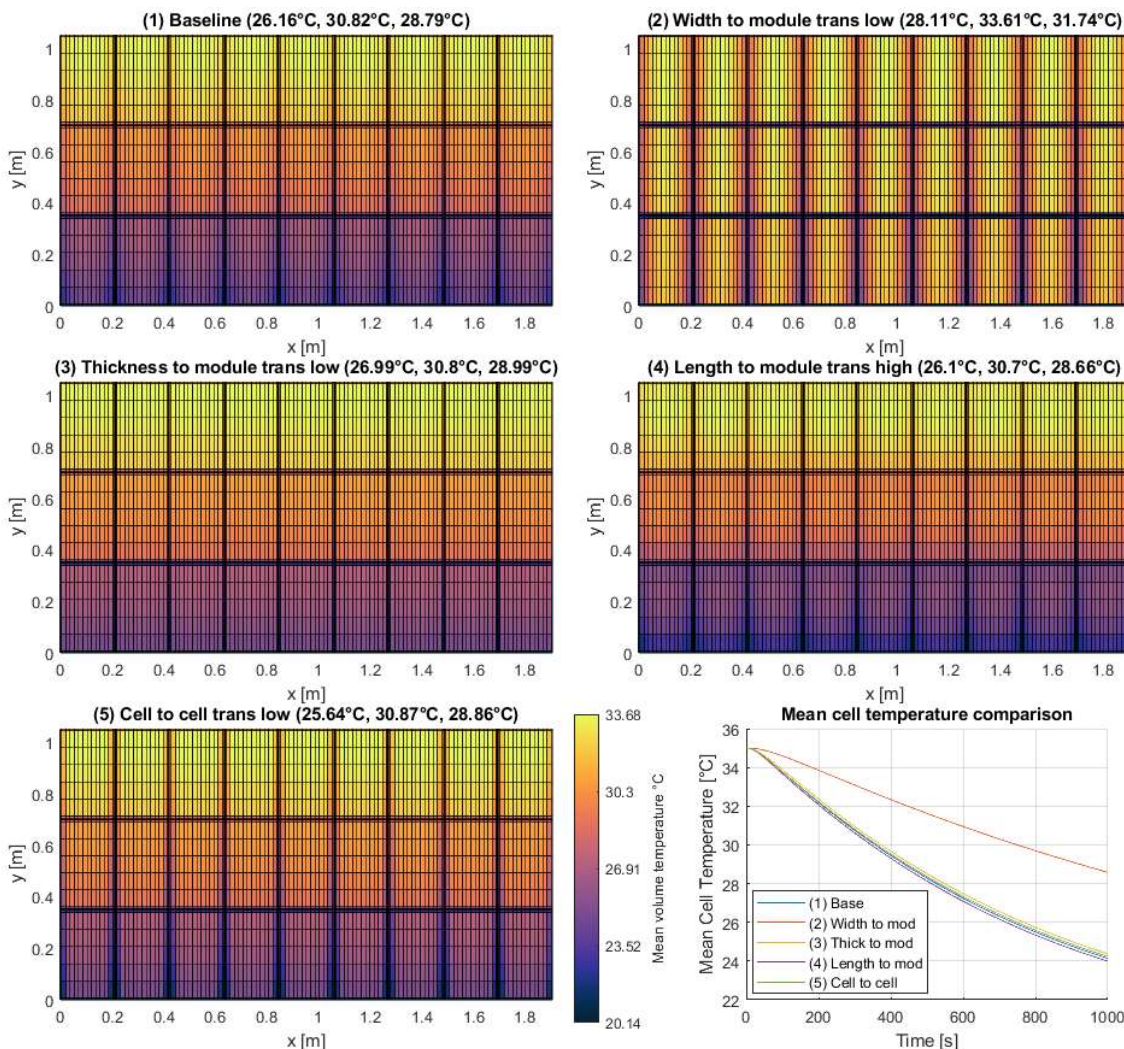
Sensitivity analysis simulations were run at a high ambient temperature (35°C) with a constant 20°C input coolant stream using the base pack layout. A constant coolant temperature input was used to keep the tests consistent and highlight changes between simulations.

7.1. Cell and module heat transfers

Figure 20 shows the results of the sensitivity analysis for the cell-cell and cell-module heat transfer, showing the mean volume temperatures with slices through the middle of the pack in the xy plane as well as a mean cell temperature comparison. For this, the conductivities were set to the opposite value compared to the initial configuration, for example, the cell width to module conductivity is set to 1 initially, so 0 is tested here.

There are only minor differences between all but the width heat transfer simulation. This is due to the orientation of the cells, most heat transfer from the cells to the modules is in the width direction as the bottom module plate is cooled directly. As the heat transfer in the length direction is low, almost all heat transfer from cells to the module must occur in the thickness direction, heavily reducing the cooling performance. The cooling reduction is shown in the mean cell temperature comparison. Additionally, as all cooling occurs via the cells on the module boundaries, large temperature gradients are produced throughout the cell stacks. If the cell orientation is changed, the balance of parameter importance would also change here.

Figure 19: Cell to module and cell to cell heat transfer sensitivity analysis results (min, max, mean cell temperatures)



7.2. Coolant thickness, heat transfer from modules and flow rate

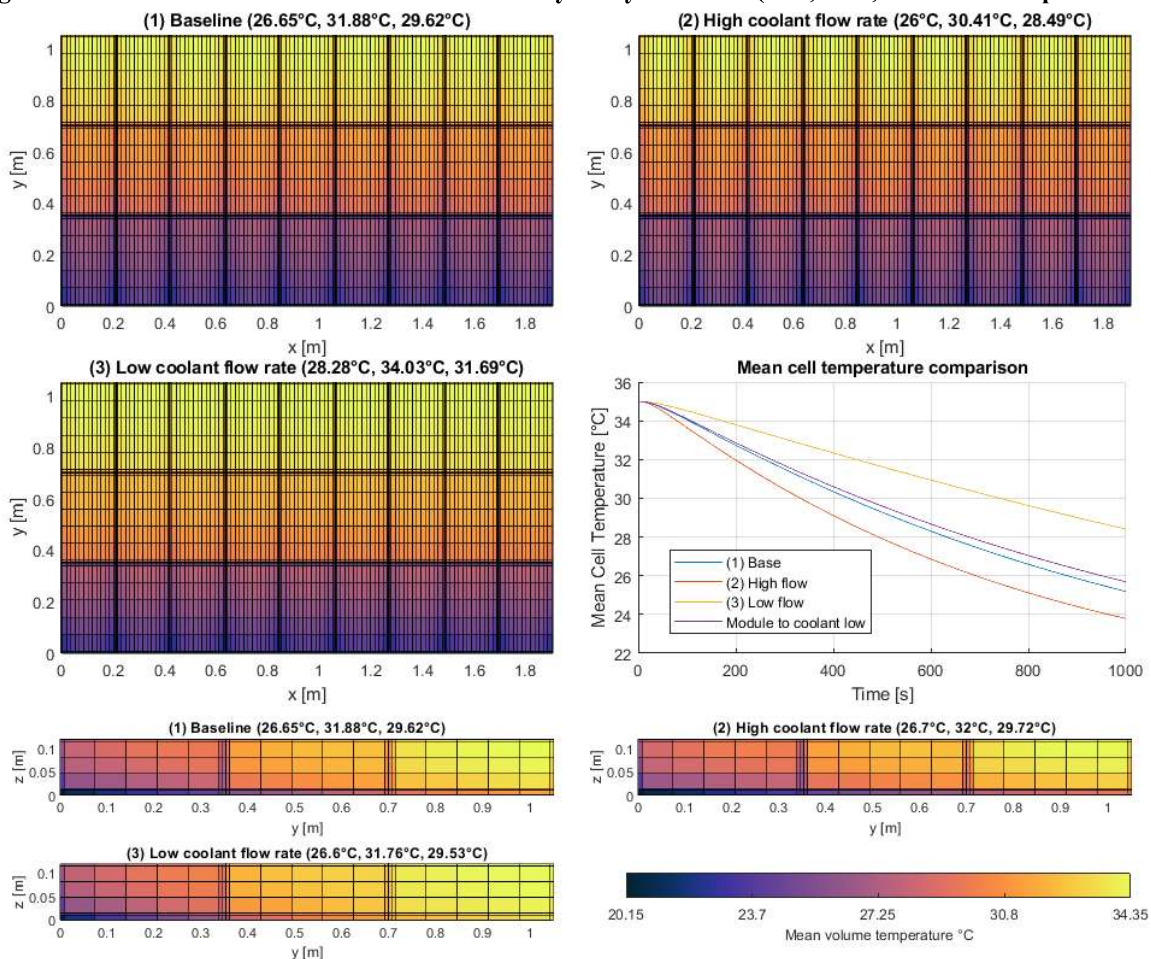
Initially, coolant thickness and heat transfer to the coolant were varied from 50 – 150% of the original values, 5 – 15mm and $1.75 - 5.25 \text{ W m}^{-1} \text{ K}^{-1}$. When the coolant thickness is reduced, the maximum flow for simulation stability is also reduced. For a fair comparison, a flow value of 0.5 kg s^{-1} was used, this is below both maximum values.

It was apparent that the coolant thickness and heat transfer had a small effect on the cooling performance of the pack, the largest change being $\sim 0.5^\circ\text{C}$ for the reduced heat transfer after a 1000s cycle. This suggested that the coolant flow rate was the limiting factor for the cooling capacity of the system in this configuration. To investigate this an additional sensitivity analysis was completed, varying the coolant flow rate from 0.25 kg s^{-1} to 0.75 kg s^{-1} .

Figure 21 shows the results of this analysis, both the xy and yz planes are included as the temperature gradients in both planes are heavily influenced by the coolant flow. The mean cell temperature figure includes the reduced heat transfer simulation as a comparison, showing the coolant flow is a much more influential factor in the cooling performance.

As expected, increasing the coolant flow improves the cooling performance of the pack as the heat transfer out of the pack is directly proportional to the flow rate at a constant temperature differential. Additionally, as more heat can be dissipated, cells further down the coolant channel can be cooled more effectively, reducing the magnitude of temperature gradients. The mean difference between minimum and maximum cell temperature for the base, high flow and low flow cases are 2.97°C , 2.49°C and 3.41°C respectively. Flow rate is the key factor in this case; however, this may change in a different configuration so the other discussed parameters should not be ignored when parameterising the model.

Figure 20: Coolant flow and heat transfer sensitivity analysis results (min, max, mean cell temperatures)



*Automotive Engineering MEng; B723936; Project supervisor: Dr Thomas Steffen

8. Future work

Due to time constraints, degradation modelling was not considered at this stage in the work. A key next step could be to implement degradation into the model. Degradation modelling can be very complex, so a simplified approach is likely desirable, such as the holistic approach used in [48]. The equations from this study could be used for a basic metric for degradation of each cell. Additionally, degradation of each cell could be used to adjust the impedance values, making the model performance more representative over long durations. If this is implemented, the user should be able to define the state of health (SOH) of each cell during initialisation. This would allow short simulations to be completed comparing the thermal performance of the pack at different SOH values.

For improved performance of the order reduction model, a wider dataset should be gathered for the PCA. This should include all cooling methods at varying ambient temperatures to cover the full range of pack performance. Additionally, an investigation into the effects of changing the number of modes in the PCA could be beneficial.

A key stage not considered in this work is the validation of the thermal model with real data. This could be completed in stages, starting with cell level, and progressing to pack level. Parameters in the initialisation can be varied to fit the model performance to the data, using the sensitivity analysis as a guideline for this process.

Finally, a library implementation would allow simple use of the pack model within wider system level models. The library should take coolant temperature, coolant flow rate and a target velocity or power demand as inputs and output cell temperatures and output coolant temperature.

9. Conclusions

A single core aim and five additional objectives in order of priority were created to monitor progress of the work. The first objective was to create a base pack model that allows the implementation of the order reduction method. An electrical and thermal battery pack model was produced in a robust way, providing good data for the order reduction stage. The second objective was to produce an initialisation script that configured the base model based on user inputs. An extensive 950 line initialisation script was produced to allow a wide array of model configurations based on user inputs, providing functionality for current work as well as potential future work. The next objective involved producing a reduced order model with reasonable accuracy allowing for real-time simulation. A reduced order model was produced, allowing for faster simulations. The real-time target was met for the default and reduced order models, with the default and reduced order models running at 34 and 169 times real-time respectively. The accuracy of the order reduction model was very good inside the passive cooling region of operation, however the accuracy greatly reduced during active cooling, these are still promising results, and the active cooling issue has been highlighted as a key area of future work. Next, a sensitivity analysis was to be completed to identify key areas for parameterisation. For the base layout, coolant flow rate and heat transfer from the cells to the cooled module face were identified as the most important factors for parameterisation. The final objective was to implement degradation into the model, however, due to time constraints degradation modelling was omitted for this work. Although degradation has not been considered the next steps for this have been outlined in the future work.

Overall, the core aim to produce a robust full-scale electrical and thermal battery pack model has been achieved. Providing a base model with the capability to be used in a wide array of future work as well as promising initial order reduction results.

10. References

- [1] 'COP26 declaration on accelerating the transition to 100% zero emission cars and vans', GOV.UK. [https://www.gov.uk/government/publications/cop26-declarationzero-emission-cars-and-vans/cop26-declaration-on-accelerating-the-transition-to-100-zero-emission-cars-and-vans](https://www.gov.uk/government/publications/cop26-declaration-zero-emission-cars-and-vans/cop26-declaration-on-accelerating-the-transition-to-100-zero-emission-cars-and-vans) (accessed May 25, 2022).
- [2] 'Government funding targeted at more affordable zero-emission vehicles as market charges ahead in shift towards an electric future', GOV.UK. <https://www.gov.uk/government/news/government-funding-targeted-at-more-affordable-zero-emission-vehicles-as-market-charges-ahead-in-shift-towards-an-electric-future> (accessed May 25, 2022).
- [3] M. S. Ziegler and J. E. Trancik, 'Re-examining rates of lithium-ion battery technology improvement and cost decline', *Energy Environ. Sci.*, vol. 14, no. 4, pp. 1635–1651, 2021, doi: 10.1039/D0EE02681F.
- [4] M. Alipour, C. Ziebert, F. V. Conte, and R. Kizilel, 'A Review on Temperature-Dependent Electrochemical Properties, Aging, and Performance of Lithium-Ion Cells', *Batteries*, vol. 6, no. 3, Art. no. 3, Sep. 2020, doi: 10.3390/batteries6030035.
- [5] G. M. Cavalheiro, T. Iriyama, G. J. Nelson, S. Huang, and G. Zhang, 'Effects of Nonuniform Temperature Distribution on Degradation of Lithium-Ion Batteries', *J. Electrochem. Energy Convers. Storage*, vol. 17, no. 2, Nov. 2019, doi: 10.1115/1.4045205.
- [6] B. Lei, W. Zhao, C. Ziebert, N. Uhlmann, M. Rohde, and H. J. Seifert, 'Experimental Analysis of Thermal Runaway in 18650 Cylindrical Li-Ion Cells Using an Accelerating Rate Calorimeter', *Batteries*, vol. 3, no. 2, Art. no. 2, Jun. 2017, doi: 10.3390/batteries3020014.
- [7] B. Shabani and M. Biju, 'Theoretical Modelling Methods for Thermal Management of Batteries', *Energies*, vol. 8, no. 9, Art. no. 9, Sep. 2015, doi: 10.3390/en80910153.
- [8] F. He, X. Li, and L. Ma, 'Combined experimental and numerical study of thermal management of battery module consisting of multiple Li-ion cells', *Int. J. Heat Mass Transf.*, vol. 72, pp. 622–629, May 2014, doi: 10.1016/j.ijheatmasstransfer.2014.01.038.
- [9] G. Karimi and X. Li, 'Thermal management of lithium-ion batteries for electric vehicles', *Int. J. Energy Res.*, vol. 37, no. 1, pp. 13–24, 2013, doi: 10.1002/er.1956.
- [10] R. Eymard, T. Gallouët, and R. Herbin, 'Finite volume methods', in *Handbook of Numerical Analysis*, vol. 7, Elsevier, 2000, pp. 713–1018. doi: 10.1016/S1570-8659(00)07005-8.
- [11] M. Keyser *et al.*, 'Enabling fast charging – Battery thermal considerations', *J. Power Sources*, vol. 367, pp. 228–236, Nov. 2017, doi: 10.1016/j.jpowsour.2017.07.009.
- [12] 'Thermal behavior of full-scale battery pack based on comprehensive heat-generation model'. <https://www.sciencedirect.com/science/article/pii/S037877531930686X> (accessed Jan. 05, 2022).
- [13] 'The Engineering ToolBox'. <https://www.engineeringtoolbox.com/> (accessed May 23, 2022).
- [14] 'Metals and Alloys - Densities'. https://www.engineeringtoolbox.com/metal-alloys-densities-d_50.html (accessed Apr. 29, 2022).
- [15] 'Metals, Metallic Elements and Alloys - Thermal Conductivities'. https://www.engineeringtoolbox.com/thermal-conductivity-metals-d_858.html (accessed Apr. 29, 2022).
- [16] 'Ethylene Glycol Heat-Transfer Fluid Properties'. https://www.engineeringtoolbox.com/ethylene-glycol-d_146.html (accessed Apr. 29, 2022).
- [17] 'Audi e-tron battery :: electricasgoneaudi.net'. <https://electricasgoneaudi.net/models/e-tron/drivetrain/battery/> (accessed Mar. 03, 2022).

- [18] S. Balkur, N. Roy Chowdhury, J. Groot, and T. Thiringer, ‘A cost and time effective novel methodology to determine specific heat capacity of lithium-ion cells’, *J. Power Sources*, vol. 500, p. 229981, Jul. 2021, doi: 10.1016/j.jpowsour.2021.229981.
- [19] T. S. Bryden *et al.*, ‘Methodology to determine the heat capacity of lithium-ion cells’, *J. Power Sources*, vol. 395, pp. 369–378, Aug. 2018, doi: 10.1016/j.jpowsour.2018.05.084.
- [20] L. Sheng, L. Su, and H. Zhang, ‘Experimental determination on thermal parameters of prismatic lithium ion battery cells’, *Int. J. Heat Mass Transf.*, vol. 139, pp. 231–239, Aug. 2019, doi: 10.1016/j.ijheatmasstransfer.2019.04.143.
- [21] M. Steinhardt, E. I. Gillich, M. Stiegler, and A. Jossen, ‘Thermal conductivity inside prismatic lithium-ion cells with dependencies on temperature and external compression pressure’, *J. Energy Storage*, vol. 32, p. 101680, Dec. 2020, doi: 10.1016/j.est.2020.101680.
- [22] S. Nejad, D. T. Gladwin, and D. A. Stone, ‘A systematic review of lumped-parameter equivalent circuit models for real-time estimation of lithium-ion battery states’, *J. Power Sources*, vol. 316, pp. 183–196, Jun. 2016, doi: 10.1016/j.jpowsour.2016.03.042.
- [23] S. Liu, J. Jiang, W. Shi, Z. Ma, L. Y. Wang, and H. Guo, ‘Butler–Volmer-Equation-Based Electrical Model for High-Power Lithium Titanate Batteries Used in Electric Vehicles’, *IEEE Trans. Ind. Electron.*, vol. 62, no. 12, pp. 7557–7568, Dec. 2015, doi: 10.1109/TIE.2015.2449776.
- [24] T. Steffen, ‘Exploring Thermal Ageing Instabilities in Lithium-Ion Batteries Using Control Oriented Cell Models’, *SAE Tech. Pap. 2022 DRAFT*.
- [25] S. Thomas, A. Fly, M. Bilal, M. Sarmiento-Carnevali, and T. Steffen, ‘Thermal management of an electric vehicle with solid-state batteries’, *[Draft]*.
- [26] J. Meng, G. Luo, M. Ricco, M. Swierczynski, D.-I. Stroe, and R. Teodorescu, ‘Overview of Lithium-Ion Battery Modeling Methods for State-of-Charge Estimation in Electrical Vehicles’, *Appl. Sci.*, vol. 8, no. 5, Art. no. 5, May 2018, doi: 10.3390/app8050659.
- [27] A. J. Smith, J. C. Burns, S. Trussler, and J. R. Dahn, ‘Precision Measurements of the Coulombic Efficiency of Lithium-Ion Batteries and of Electrode Materials for Lithium-Ion Batteries’, *J. Electrochem. Soc.*, vol. 157, no. 2, p. A196, Dec. 2009, doi: 10.1149/1.3268129.
- [28] ‘BMW Gen5 High-Voltage-Battery for BMW iX3’. <https://www.press.bmwgroup.com/global/photo/detail/P90392467/bmw-gen5-high-voltage-battery-for-bmw-ix3?language=en> (accessed May 23, 2022).
- [29] ‘New Jaguar I-Pace’s battery electric vehicle technology at a glance’, *Autocar*. <https://www.autocar.co.uk/car-news/motor-shows-la-motor-show/new-jaguar-i-pace%20%80%99s-battery-electric-vehicle-technology-glance> (accessed May 23, 2022).
- [30] ‘What we know about the Volkswagen ID.4 Battery Pack - GoSaveTime Green Technology’. <https://gosavetime.com/what-we-know-about-the-volkswagen-id-4-battery-pack> (accessed May 23, 2022).
- [31] B. Crothers, ‘Chevy Bolt EV Battery Issues And Fire Risk: Two Cases’, *Forbes*. <https://www.forbes.com/sites/brookecrothers/2021/05/09/chevy-bolt-ev-battery-issues-and-fire-risk-two-cases/> (accessed May 23, 2022).
- [32] H. Abdi and L. J. Williams, ‘Principal component analysis’, *WIREs Comput. Stat.*, vol. 2, no. 4, pp. 433–459, 2010, doi: 10.1002/wics.101.
- [33] M. Vyas, K. Pareek, S. Spare, A. Garg, and L. Gao, ‘State-of-charge prediction of lithium ion battery through multivariate adaptive recursive spline and principal component analysis’, *Energy Storage*, vol. 3, no. 2, p. e147, 2021, doi: 10.1002/est2.147.
- [34] J. Guo and Z. Li, ‘Prognostics of Lithium ion battery using functional principal component analysis’, in *2017 IEEE International Conference on Prognostics and Health Management (ICPHM)*, Jun. 2017, pp. 14–17. doi: 10.1109/ICPHM.2017.7998299.
- [35] ‘Principal component analysis of raw data - MATLAB pca - MathWorks United Kingdom’. <https://uk.mathworks.com/help/stats/pca.html> (accessed May 20, 2022).

- [36] SJThomas29, *SJThomas29/Reduced-Order-Thermal-Simulation-of-Lithium-Ion-Battery-Packs*. 2022. Accessed: May 25, 2022. [Online]. Available: <https://github.com/SJThomas29/Reduced-Order-Thermal-Simulation-of-Lithium-Ion-Battery-Packs>
- [37] ‘2021 Audi e-tron 50 quattro - Specifications’, *EVSPECIFICATIONS*. <https://www.evspecifications.com/en/model/be5f196> (accessed May 02, 2022).
- [38] L. Zhang, H. Peng, Z. Ning, Z. Mu, and C. Sun, ‘Comparative Research on RC Equivalent Circuit Models for Lithium-Ion Batteries of Electric Vehicles’, *Appl. Sci.*, vol. 7, no. 10, Art. no. 10, Oct. 2017, doi: 10.3390/app7101002.
- [39] ‘Differential Equations - The Heat Equation’. <https://tutorial.math.lamar.edu/classes/de/theheatequation.aspx> (accessed Apr. 27, 2022).
- [40] ‘Metals - Specific Heats’. https://www.engineeringtoolbox.com/specific-heat-metals-d_152.html (accessed Apr. 29, 2022).
- [41] ‘How battery pack heat management enhance performances of EV? || Elkem Silicones’, *Elkem.com*. <https://www.elkem.com/silicones/blog/industrial-assembly-electronic-protection/battery-pack-heat-management-hev-battery/> (accessed May 01, 2022).
- [42] K. Darcovich, D. D. MacNeil, S. Recoskie, Q. Cadic, and F. Ilinca, ‘Comparison of cooling plate configurations for automotive battery pack thermal management’, *Appl. Therm. Eng.*, vol. 155, pp. 185–195, Jun. 2019, doi: 10.1016/j.applthermaleng.2019.03.146.
- [43] ‘Henkel in the Automotive Industry’. <https://www.henkel-adhesives.com/at/en/industries/automotive.html> (accessed May 11, 2022).
- [44] ‘whitepaper-bergquist-liqui-form-tlf-3500cgel.pdf’. Accessed: May 11, 2022. [Online]. Available: <https://dm.henkel-dam.com/is/content/henkel/whitepaper-bergquist-liqui-form-tlf-3500cgel>
- [45] D. Leighton, ‘Combined Fluid Loop Thermal Management for Electric Drive Vehicle Range Improvement’, *SAE Int. J. Passeng. Cars - Mech. Syst.*, vol. 8, no. 2, pp. 711–720, Apr. 2015, doi: 10.4271/2015-01-1709.
- [46] D. Jung and D. N. Assanis, ‘Numerical Modeling of Cross Flow Compact Heat Exchanger with Louvered Fins using Thermal Resistance Concept’, SAE International, Warrendale, PA, SAE Technical Paper 2006-01-0726, Apr. 2006. doi: 10.4271/2006-01-0726.
- [47] ‘Electric Vehicle Thermal Management - MATLAB & Simulink - MathWorks United Kingdom’. https://uk.mathworks.com/help/physmod/hydro/ug/sscfluids_ev_thermal_management.html?searchHighlight=ev%20cooling&s_tid=srchtitle_ev%20cooling_6 (accessed May 13, 2022).
- [48] J. Schmalstieg, S. Käbitz, M. Ecker, and D. U. Sauer, ‘A holistic aging model for Li(NiMnCo)O₂ based 18650 lithium-ion batteries’, *J. Power Sources*, vol. 257, pp. 325–334, Jul. 2014, doi: 10.1016/j.jpowsour.2014.02.012.